ACS OMEGA

http://pubs.acs.org/journal/acsodf

Article

Design, Microwave-Assisted Synthesis, Antimicrobial and Anticancer Evaluation, and *In Silico* Studies of Some 2-Naphthamide Derivatives as DHFR and VEGFR-2 Inhibitors

Em Canh Pham* and Tuyen Ngoc Truong*

Cite This: *ACS Omega* 2022, 7, 33614–33628

Read Online

ACCESS | Metrics & More | Article Recommendations | Supporting Information

ABSTRACT: Naphthamide is a common structural framework with diverse pharmacological activities. Ten novel 2-naphthamide derivatives have been designed, synthesized, and evaluated for their *in vitro* antibacterial, antifungal, and anticancer activities. The title compounds were synthesized from dimethoxybenzaldehyde derivatives through a four-step microwave-assisted synthesis process. The structures were confirmed by ^{1}H NMR, ^{13}C NMR, and MS spectra. Compound **8b** showed good antibacterial activity against *Escherichia coli*, *Streptococcus faecalis*, *Salmonella enterica*, MSSA, and MRSA with MIC values of 16, 16, 16, 8, and 16 μg/mL, respectively, compared to ciprofloxacin (MIC = 8−16 μg/mL). Compounds **5b** (IC_{50} = 3.59−8.38 μM) and **8b** (IC_{50} = 2.97−7.12 μM) exhibited good cytotoxic activity against C26, HepG2, and MCF7 cancer cell lines as compared to paclitaxel (IC_{50} = 2.85−5.75 μM). Moreover, compounds **5b** and **8b** exhibited better anticancer activity than PTX against the C26 cell line. In particular, compound **8b** showed potent *in vitro* VEGFR-2 inhibitory activity with the IC_{50} value of 0.384 μM compared with sorafenib (IC_{50} = 0.069 μM). Therefore, compound **8b** is the most potent compound for anticancer activity as indicated by *in vitro* cell line inhibition, *in silico* ADMET, molecular docking, and *in vitro* VEGFR-2 inhibition studies.

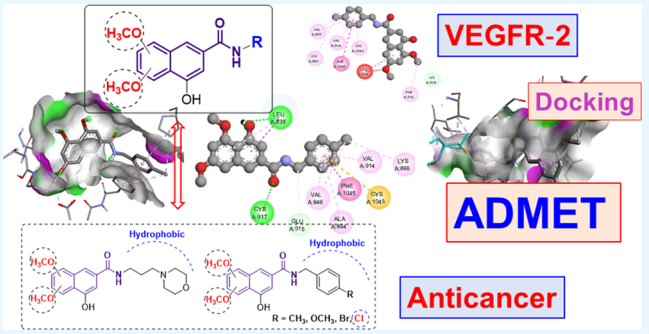

1. INTRODUCTION

Bacterial and fungal resistance can cause life-threatening diseases. In addition, cancer drug resistance is also expanding and posing a great threat to human health and life. This has resulted in research and development in search of new antibiotics and anticancer drugs to maintain an effective drug supply at all times.[1−4] Besides, the commonly used antibacterial drugs such as amoxicillin, norfloxacin, and ciprofloxacin as well as the commonly used antifungal drugs such as clotrimazole, fluconazole, amphotericin, and nystatin are related to severe side effects. Moreover, anticancer drugs including vinca alkaloids (e.g., vinblastine and vincristine) and taxanes (e.g., paclitaxel and docetaxel) always have limited clinical use due to side effects, such as poor solubility, low oral bioavailability, high toxicity, the development of drug resistance, and complex synthesis.[5,6] Therefore, it is important to find out newer, safer, and more effective antibiotics and anticancer drugs with multiple effects, especially showing both good anticancer and antimicrobial activities. This is very beneficial for cancer patients due to their weakened immunity and susceptibility to microbial attack.

Naphthalene is the simplest polycyclic aromatic hydrocarbon consisting of a fused pair of benzene rings. On the other hand, naphthamide derivatives containing a naphthalene nucleus are a common structural framework in various biologically active natural products, pharmaceuticals, and materials.[7,8] In addition, the naphthamide derivatives showed a large spectrum of activities in various pharmacological fields like anticancer,[9−12] antibacterial,[13−15] antifungal,[15−17] anti-inflammatory,[18] and antioxidants.[19] Moreover, many important drugs used therapeutically in the research area contain naphthalene moieties such as nafcillin, bedaquiline, naproxen, tolnaftate, duloxetine, and propanolol (Figure 1).

Dihydrofolate reductase receptor (DHFR) and vascular endothelial growth factor receptor 2 (VEGFR-2) are important targets in the design and development of novel antitumor agents. In addition, DHFR is also used in the design of antibacterial and antifungal agents. Inhibition of DHFR leads to a decrease in intracellular folate required for one carbon transformation and is therefore important for the biosynthesis of thymidylate, purine nucleotide, methionine, and many other compounds required for RNA and DNA biosynthesis. Furthermore, this receptor has a high binding affinity and selectivity for co-substrates, making it difficult to be displaced by natural substrates.[1,20] On the other

Received: August 13, 2022
Accepted: August 31, 2022
Published: September 9, 2022

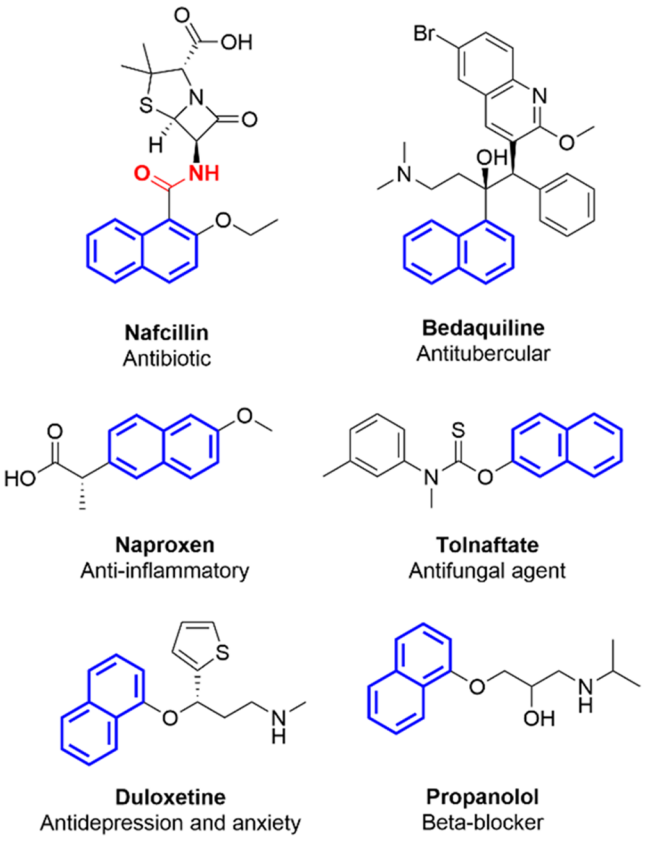

Figure 1. Marketed naphthalene ring containing drug compounds.

hand, VEGFR-2 is strongly associated with poor prognosis and tumor metastasis. VEGFR-2-mediated signaling promotes a number of endothelial responses required for the formation of new blood vessels, such as cell proliferation, metastasis, and survival of cancer cells.[21,22]

1.1. Rationale and Structure-Based Design as Antimicrobial and Anticancer Agents. Structure−activity relationship studies of the naphthalene ring system suggested that the C-1 and C-2 positions are very much important for the pharmacological effect.[12] Especially, naphthamide derivatives are potent VEGFR-2 inhibitors, for example, amide groups similar to anticancer drugs (sorafenib, sunitinib, pazopanib, axitinib, vandetanib, and regorafenib). Our designed derivatives and anticancer drug millepachine (potent cytotoxicity against a variety of human cancer cells with an IC_{50} range of 0.76−4.66 μM), linifanib, and derivatives of Harmange et al., and Lv et al., share three common essential structural features such as a planar naphthalene moiety, the amide group at C-1 and C-2 positions, and the −OR-substituted groups at different positions (Figure 2).[12,23]

Therefore, the purpose of this study is to synthesize novel *N*-(4-substituted benzyl) and *N*-(3-morpholinopropyl) 2-naphthamide derivatives with dimethoxy substituents at positions 5,7 and 6,8 as well as different NH-substituted groups and evaluate their antibacterial, antifungal, and anticancer activities. The active derivatives will be subjected to molecular docking studies to understand potential drug−receptor interactions and the *in silico* ADMET pharmacokinetic profile as well as to evaluate *in vitro* DHFR and VEGFR-2 inhibitory activities.

2. EXPERIMENTAL SECTION

2.1. Materials. All reagents and chemicals were obtained from the commercial supplier Merck (Germany) and used without further purification. Reactions were monitored by thin-layer chromatography (TLC) carried out on silica gel plates (E-Merck Kieselgel 60 F_{254}) using UV light as the visualizing agent. Silica gel (0.040−0.063 mm) from Merck (Germany) was used for column chromatography.

The microwave-assisted synthesis was performed by a microwave synthesizer (CEM Discover) with continuous stirring and infrared temperature sensors. Melting points (mp, °C) were determined in an open capillary using a Gallenkamp melting point apparatus (Sanyo Gallenkamp, U.K.). A Shimadzu FTIR (IRAffinity-1S) spectrometer was used to record the infrared (IR) spectra. Nuclear magnetic resonance (^{1}H NMR and ^{13}C NMR) spectra were recorded on a Bruker Avance 500 (^{1}H, 500 MHz; ^{13}C, 125 MHz) NMR spectrometer at ambient temperature using $CDCl_3$ and DMSO-d_6 as solvents. Chemical shifts are reported in parts per million (ppm) relative to the residual solvent peak as following: $CDCl_3$ = 7.26 ppm (^{1}H NMR), DMSO-d_6 = 2.50 ppm (^{1}H NMR), $CDCl_3$ = 77.16 ppm (^{13}C NMR), and DMSO-d_6 = 40.00 ppm (^{13}C NMR). A liquid chromatography machine (Agilent Technologies 1100 series LC/MSD Trap) was used to record the mass spectra (MS). Optical density (OD) was measured at 570 nm on a Multiskan microplate reader.

2.2. Experimental Procedures. *2.2.1. General Procedure for the Preparation of (E)-4-(2,4 or 3,5-Dimethoxyphenyl)-3-(ethoxycarbonyl)but-3-enoic Acid (**1a**−**1b**).* A mixture of diethyl succinate (10 mmol), 2,4 or 3,5-dimethoxybenzaldehyde (5 mmol), potassium *tert*-butoxide (*t*-BuOK, 10 mmol), and *tert*-butanol (*t*-BuOH, 10 mL) was dissolved in a sealed reactor vessel. The reaction mixture was microwave-irradiated for 15 min at 60 °C with 200 W energy and a high stirring speed. When the reaction was complete, the mixture was acidified with acetic acid, and then the product was extracted with ethyl acetate. After removing the solvent, a brown crude product was obtained. The pure yellow crystals were obtained by column chromatography on silica gel with hexane and ethyl acetate (5:1 v/v) as the mobile phase. Reaction yields obtained range from 92 to 94%.

*2.2.2. General Procedure for the Preparation of Ethyl 4-Acetoxy-6,8 or 5,7-Dimethoxy-2-naphthoate (**2a**−**2b**).* A mixture of compound **1** (1 mmol), sodium acetate (NaOAc, 1 mmol), and acetic anhydride (Ac_2O, 5 mmol) was dissolved in a sealed reactor vessel. The reaction mixture was microwave irradiated for 10 min at 130 °C with 300 W energy and a high stirring speed. When the reaction was complete, the mixture was cooled, and then 15% NaOH solution was added to neutralize the excess acid. The product was extracted with ethyl acetate, and the solvent was evaporated to yield the crude product. The pure white crystals were obtained by column chromatography on silica gel with hexane and ethyl acetate (6:1 v/v) as the mobile phase. Reaction yields obtained range from 91 to 93%.

*2.2.3. General Procedure for the Preparation of 4-Hydroxy-6,8 or 5,7-Dimethoxynaphthalene-2-carboxylic Acid (**3a**−**3b**).* A mixture of compound **2** (5 mmol), 3M KOH solution (5 mL), and 95% ethanol (EtOH, 5 mL) was dissolved in a sealed reactor vessel. The reaction mixture was microwave irradiated for 15 min at 80 °C with 300 W energy and a high stirring speed. When the reaction was complete, the mixture was neutralized with a 10% HCl solution. The product was extracted with ethyl acetate, and the solvent was evaporated to yield the crude

https://doi.org/10.1021/acsomega.2c05206
ACS Omega 2022, 7, 33614−33628

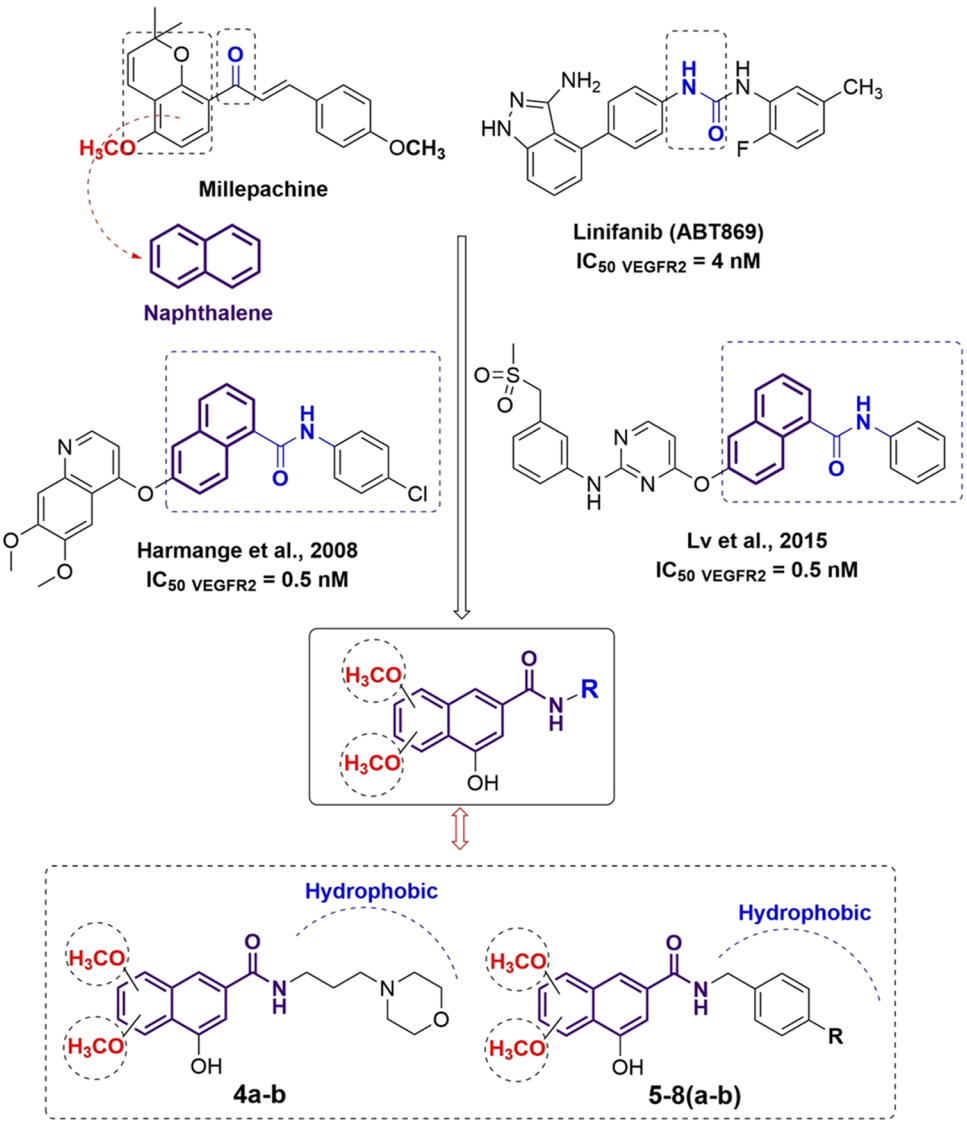

Figure 2. Rational study design, illustrating the structure of the newly designed *N*-(4-substituted benzyl) and *N*-(3-morpholinopropyl) 2-naphthamide derivatives with representative examples for anticancer compounds (IC_{50}, half-maximal inhibitory concentration; VEGFR, vascular endothelial growth factor receptor).

product. The pure yellow crystals were obtained by column chromatography on silica gel with hexane and ethyl acetate (3:1 v/v) as the mobile phase. Reaction yields obtained range from 95 to 96%.

*2.2.4. General Procedure for the Preparation of N-(4-Substituted benzyl) and N-(3-Morpholinopropyl) 2-Naphthamide Derivatives (**4a−4b** and **5−8(a−b)**). 2.2.4.1. Reflux Method.* To a mixture of compound **3** (1 mmol) and acetonitrile (MeCN, 20 mL) was added drop by drop of thionyl chloride ($SOCl_2$, 5 mL). The reaction mixture was stirred in a nitrogen atmosphere at room temperature for 3.5 h. After removing the solvent, the solid was redissolved in acetonitrile (10 mL) and then gradually added 3-morpholinopropylamine or 4-substituted benzylamine (3 mmol) to the reaction flask and continued stirring the mixture in nitrogen gas at room temperature for 5 min. The product was extracted with ethyl acetate, and the solvent was evaporated to yield the crude product. The pure white crystals were obtained by column chromatography on silica gel with ethyl acetate and methanol (6:1 v/v) as the mobile phase. Reaction yields obtained range from 80 to 86%.

2.2.4.2. Microwave-Assisted Method. A mixture of compound **3** (1 mmol) and acetonitrile (MeCN, 20 mL) was dissolved in a sealed reactor vessel. To the mixture was added drop by drop of thionyl chloride ($SOCl_2$, 5 mL) and irradiated for 30 min at 80 °C with a power of 300 W. After removing the solvent, the solid was redissolved in acetonitrile (10 mL) and then added 3-morpholinopropylamine or 4-substituted benzylamine (3 mmol) and continued to irradiate for 2 min at 130 °C with 300 W energy and a high stirring speed. The product was extracted with ethyl acetate, and the solvent was evaporated to yield the crude product. The pure white crystals were obtained by column chromatography on silica gel with ethyl acetate and methanol (6:1 v/v) as the mobile phase. Reaction yields obtained range from 93 to 97%.

*2.2.5. (E)-4-(2,4-dimethoxyphenyl)-3-(ethoxycarbonyl)-but-3-enoic Acid (**1a**).* Yellow solid, mp 116−117 °C. ^{1}H NMR (500 MHz, $CDCl_3$, δ ppm): 7.98 (1H, s, -CH═C-), 7.27 (1H, s, H_{Ar}), 6.54 (1H, d, J = 2.0 Hz, H_{Ar}), 6.47 (1H, d, J = 2.0 Hz, H_{Ar}), 4.29 (2H, q, J = 7.0 Hz, -CH_2-OCO-), 3.83 (3H, s, -OCH_3), 3.75 (3H, s, -OCH_3), 3.52 (2H, s, -CH_2-COOH), 1.35

https://doi.org/10.1021/acsomega.2c05206
ACS Omega 2022, 7, 33614−33628

(3H, t, J = 7.0 Hz, -CH_3). ^{13}C NMR (125 MHz, $CDCl_3$, δ ppm): 168.0, 162.1, 159.0, 138.4, 130.8, 123.7, 116.6, 110.0, 104.6, 98.5, 61.6, 56.5, 55.5, 34.2, 14.2. LC-MS (m/z) $[M - H]^-$ calcd for $C_{15}H_{17}O_6$ 293.1031, found 293.1039.

*2.2.6. (E)-4-(3,5-dimethoxyphenyl)-3-(ethoxycarbonyl)-but-3-enoic Acid (**1b**).* Yellow solid, mp 118−119 °C. ^{1}H NMR (500 MHz, $CDCl_3$, δ ppm): 7.96 (1H, s, -CH═C-), 7.28 (1H, s, H_{Ar}), 6.55 (1H, d, J = 1.5 Hz, H_{Ar}), 6.44 (1H, d, J = 2.0 Hz, H_{Ar}), 4.31 (2H, q, J = 7.5 Hz, -CH_2-OCO-), 3.82 (3H, s, -OCH_3), 3.77 (3H, s, -OCH_3), 3.54 (2H, s, -CH_2-COOH), 1.36 (3H, t, J = 7.0 Hz, -CH_3). ^{13}C NMR (125 MHz, $CDCl_3$, δ ppm): 168.3, 161.9, 159.2, 138.5, 130.6, 123.8, 116.9, 110.3, 104.5, 98.6, 61.4, 56.6, 55.4, 34.3, 14.5. LC-MS (m/z) $[M - H]^-$ calcd for $C_{15}H_{17}O_6$ 293.1031, found 293.1028.

*2.2.7. Ethyl 4-Acetoxy-6,8-dimethoxy-2-naphthoate (**2a**).* White solid. ^{1}H NMR (500 MHz, $CDCl_3$, δ ppm): 8.80 (1H, d, J = 0.5 Hz, H_{Ar}), 7.81 (1H, d, J = 1.5 Hz, H_{Ar}), 6.67 (1H, d, J = 2.0 Hz, H_{Ar}), 6.54 (1H, d, J = 2.0 Hz, H_{Ar}), 4.41 (2H, q, J = 7.0 Hz, -CH_2-), 4.02 (3H, s, -OCH_3), 4.01 (3H, s, -OCH_3), 1.43 (3H, t, J = 7.0 Hz, -CH_3). ^{13}C NMR (125 MHz, $CDCl_3$, δ ppm): 169.2, 166.3, 161.0, 158.0, 145.4, 131.2, 124.5, 123.3, 122.3, 119.2, 98.6, 91.7, 61.1, 55.8, 55.4, 21.0, 14.4. LC-MS (m/z) $[M - H]^-$ calcd for $C_{17}H_{17}O_6$ 317.1031, found 317.1045; $[M + H]^+$ calcd for $C_{17}H_{19}O_6$ 319.1176, found 319.1169.

*2.2.8. Ethyl 4-Acetoxy-5,7-dimethoxy-2-naphthoate (**2b**).* White solid. ^{1}H NMR (500 MHz, $CDCl_3$, δ ppm): 8.79 (1H, d, J = 1.0 Hz, H_{Ar}), 7.86 (1H, d, J = 2.0 Hz, H_{Ar}), 6.68 (1H, d, J = 2.0 Hz, H_{Ar}), 6.53 (1H, d, J = 2.0 Hz, H_{Ar}), 4.42 (2H, q, J = 7.0 Hz, -CH_2-), 4.04 (3H, s, -OCH_3), 4.02 (3H, s, -OCH_3), 1.45 (3H, t, J = 7.0 Hz, -CH_3). ^{13}C NMR (125 MHz, $CDCl_3$, δ ppm): 169.4, 166.5, 161.1, 157.9, 145.2, 131.3, 124.7, 123.2, 122.4, 119.5, 98.5, 91.9, 61.2, 55.9, 55.5, 21.2, 14.6. LC-MS (m/z) $[M - H]^-$ calcd for $C_{17}H_{17}O_6$ 317.1031, found 317.1048; $[M + H]^+$ calcd for $C_{17}H_{19}O_6$ 319.1176, found 319.1181.

*2.2.9. 4-Hydroxy-6,8-dimethoxy-2-naphthoic Acid (**3a**).* Yellow solid. ^{1}H NMR (500 MHz, $CDCl_3$, δ ppm): 8.47 (1H, s, H_{Ar}), 7.36 (1H, d, J = 1.5 Hz, H_{Ar}), 7.14 (1H, d, J = 2.0 Hz, 1H, H_{Ar}), 6.53 (1H, d, J = 2.0 Hz, H_{Ar}), 3.98 (3H, s, -OCH_3), 3.95 (3H, s, -OCH_3). ^{13}C NMR (125 MHz, $CDCl_3$, δ ppm): 169.9, 159.8, 157.5, 151.8, 129.3, 124.1, 121.9, 117.4, 108.3, 98.4, 92.7, 55.5, 55.4. LC-MS (m/z) $[M - H]^-$ calcd for $C_{13}H_{11}O_5$ 247.0612, found 247.0653.

*2.2.10. 4-Hydroxy-5,7-dimethoxy-2-naphthoic Acid (**3b**).* Yellow solid. ^{1}H NMR (500 MHz, $CDCl_3$, δ ppm): 8.43 (1H, s, H_{Ar}), 7.34 (1H, d, J = 2.0 Hz, H_{Ar}), 7.13 (1H, d, J = 2.0 Hz, 1H, H_{Ar}), 6.56 (1H, d, J = 2.0 Hz, H_{Ar}), 3.99 (3H, s, -OCH_3), 3.96 (3H, s, -OCH_3). ^{13}C NMR (125 MHz, $CDCl_3$, δ ppm): 169.6, 159.7, 157.3, 151.9, 129.4, 124.2, 121.8, 117.5, 108.4, 98.6, 92.8, 55.7, 55.5. LC-MS (m/z) $[M - H]^-$ calcd for $C_{13}H_{11}O_5$ 247.0612, found 247.0625.

*2.2.11. 4-Hydroxy-6,8-dimethoxy-N-(3-morpholinopropyl)-2-naphthamide (**4a**).* White solid, mp 172−174 °C. ^{1}H NMR (500 MHz, DMSO-d_6, δ ppm): 8.54 (1H, s, -NH-), 8.00 (1H, s, H_{Ar}), 7.32 (1H, s, H_{Ar}), 7.04 (1H, d, J = 2.0 Hz, H_{Ar}), 6.63 (1H, d, J = 2.5 Hz, H_{Ar}), 3.96 (3H, s, -OCH_3), 3.89 (3H, s, -OCH_3), 3.58 (4H, t, J = 4.5 Hz, -CH_2-), 3.31 (2H, q, J = 6.5 Hz, -CH_2-), 2.34 (6H, t, J = 7.0 Hz, -CH_2-), 1.72−1.68 (2H, m, -CH_2-). ^{13}C NMR (125 MHz, DMSO-d_6, δ ppm): 166.9, 158.5, 156.5, 152.3, 129.8, 127.5, 121.3, 111.6, 107.9, 98.6, 92.9, 66.3, 56.4, 55.8, 55.3, 53.1, 38.4, 25.8. LC-MS (m/z) $[M - H]^-$ calcd for $C_{20}H_{25}N_2O_5$ 373.1769, found 373.1754; $[M + H]^+$ calcd for $C_{20}H_{27}N_2O_5$ 375.1914, found 375.1898.

*2.2.12. 4-Hydroxy-5,7-dimethoxy-N-(3-morpholinopropyl)-2-naphthamide (**4b**).* White solid, mp 174−175 °C. ^{1}H NMR (500 MHz, DMSO-d_6, δ ppm): 8.52 (1H, s, -NH-), 7.98 (1H, s, H_{Ar}), 7.30 (1H, s, H_{Ar}), 7.03 (1H, d, J = 2.0 Hz, H_{Ar}), 6.63 (1H, d, J = 2.5 Hz, H_{Ar}), 3.94 (3H, s, -OCH_3), 3.86 (3H, s, -OCH_3), 3.59 (4H, t, J = 4.5 Hz, -CH_2-), 3.30 (2H, q, J = 6.5 Hz, -CH_2-), 2.35 (6H, t, J = 7.0 Hz, -CH_2-), 1.71−1.67 (2H, m, -CH_2-). ^{13}C NMR (125 MHz, DMSO-d_6, δ ppm): 166.8, 158.4, 156.7, 152.2, 129.7, 127.5, 121.2, 111.4, 108.0, 98.5, 92.7, 66.2, 56.5, 55.7, 55.2, 53.4, 38.2, 25.7. LC-MS (m/z) $[M - H]^-$ calcd for $C_{20}H_{25}N_2O_5$ 373.1769, found 373.1746; $[M + H]^+$ calcd for $C_{20}H_{27}N_2O_5$ 375.1914, found 375.1901.

*2.2.13. 4-Hydroxy-6,8-dimethoxy-N-(4-methylbenzyl)-2-naphthamide (**5a**).* White solid, mp 135−136 °C. ^{1}H NMR (500 MHz, DMSO-d_6, δ ppm): 10.16 (1H, s, -OH), 9.01 (1H, s, -NH-), 8.05 (1H, d, J = 1.0 Hz, H_{Ar}), 7.33 (1H, d, J = 2.0 Hz, H_{Ar}), 7.22 (2H, d, J = 8.0 Hz, H_{Ar}), 7.12 (2H, d, J = 8.0 Hz, H_{Ar}), 7.02 (1H, d, J = 2.0 Hz, H_{Ar}), 6.65 (1H, d, J = 2.0 Hz, H_{Ar}), 4.43 (2H, d, J = 6.0 Hz, -CH_2-), 3.94 (3H, s, -OCH_3), 3.88 (3H, s, -OCH_3), 2.29 (3H, s, -CH_3). ^{13}C NMR (125 MHz, DMSO-d_6, δ ppm): 166.6, 158.5, 156.9, 152.2, 136.8, 135.5, 129.5, 128.6, 127.7, 127.3, 121.2, 111.9, 107.7, 98.6, 92.8, 55.6, 55.3, 42.2, 20.5. LC-MS (m/z) $[M - H]^-$ calcd for $C_{21}H_{20}NO_4$ 350.1398, found 350.1376; $[M + H]^+$ calcd for $C_{21}H_{22}NO_4$ 352.1543, found 352.1512.

*2.2.14. 4-Hydroxy-5,7-dimethoxy-N-(4-methylbenzyl)-2-naphthamide (**5b**).* White solid, mp 136−138 °C. ^{1}H NMR (500 MHz, DMSO-d_6, δ ppm): 10.14 (1H, s, -OH), 8.99 (1H, s, -NH-), 8.06 (1H, d, J = 1.0 Hz, H_{Ar}), 7.32 (1H, d, J = 2.0 Hz, H_{Ar}), 7.22 (2H, d, J = 8.0 Hz, H_{Ar}), 7.13 (2H, d, J = 8.0 Hz, H_{Ar}), 7.04 (1H, d, J = 2.0 Hz, H_{Ar}), 6.64 (1H, d, J = 2.0 Hz, H_{Ar}), 4.42 (2H, d, J = 6.0 Hz, -CH_2-), 3.95 (3H, s, -OCH_3), 3.87 (3H, s, -OCH_3), 2.27 (3H, s, -CH_3). ^{13}C NMR (125 MHz, DMSO-d_6, δ ppm): 166.7, 158.4, 156.7, 152.0, 137.0, 135.6, 129.4, 128.7, 127.5, 127.2, 121.2, 111.8, 107.9, 98.4, 92.6, 55.7, 55.2, 42.4, 20.6. LC-MS (m/z) $[M - H]^-$ calcd for $C_{21}H_{20}NO_4$ 350.1398, found 350.1382; $[M + H]^+$ calcd for $C_{21}H_{22}NO_4$ 352.1543, found 352.1529.

*2.2.15. 4-Hydroxy-6,8-dimethoxy-N-(4-methoxybenzyl)-2-naphthamide (**6a**).* White solid, mp 151−152 °C. ^{1}H NMR (500 MHz, DMSO-d_6, δ ppm): 10.17 (1H, s, -OH), 9.04 (1H, s, -NH-), 8.08 (1H, d, J = 1.5 Hz, H_{Ar}), 7.34 (1H, d, J = 2.0 Hz, H_{Ar}), 7.13 (2H, d, J = 7.5 Hz, H_{Ar}), 7.03 (1H, d, J = 2.0 Hz, H_{Ar}), 6.93 (2H, d, J = 8.0 Hz, H_{Ar}), 6.65 (1H, d, J = 2.0 Hz, H_{Ar}), 4.34 (2H, d, J = 6.0 Hz, -CH_2-), 3.98 (3H, s, -OCH_3), 3.93 (3H, s, -OCH_3), 3.90 (3H, s, -OCH_3). ^{13}C NMR (125 MHz, DMSO-d_6, δ ppm): 167.0, 158.7, 156.9, 154.4, 152.3, 136.9, 135.4, 129.8, 128.6, 127.7, 127.3, 112.3, 107.7, 98.7, 92.8, 55.6, 55.3, 43.2. LC-MS (m/z) $[M - H]^-$ calcd for $C_{21}H_{20}NO_4$ 366.1347, found 366.1368; $[M + H]^+$ calcd for $C_{21}H_{22}NO_4$ 368.1492, found 368.1487.

*2.2.16. 4-Hydroxy-5,7-dimethoxy-N-(4-methoxybenzyl)-2-naphthamide (**6b**).* White solid, mp 154−155 °C. ^{1}H NMR (500 MHz, DMSO-d_6, δ ppm): 10.14 (1H, s, -OH), 9.01 (1H, s, -NH-), 8.09 (1H, d, J = 2.0 Hz, H_{Ar}), 7.33 (1H, d, J = 2.0 Hz, H_{Ar}), 7.13 (2H, d, J = 8.0 Hz, H_{Ar}), 7.04 (1H, d, J = 2.0 Hz, H_{Ar}), 6.93 (2H, d, J = 8.0 Hz, H_{Ar}), 6.66 (1H, d, J = 2.0 Hz, H_{Ar}), 4.33 (2H, d, J = 6.0 Hz, -CH_2-), 3.99 (3H, s, -OCH_3), 3.92 (3H, s, -OCH_3), 3.88 (3H, s, -OCH_3). ^{13}C NMR (125 MHz, DMSO-d_6, δ ppm): 166.8, 159.0, 156.8, 155.0, 153.0, 137.3, 135.9, 129.5, 128.6, 127.5, 127.4, 112.7, 107.9, 98.6, 92.7, 56.0, 55.5, 42.1. LC-MS (m/z) $[M - H]^-$ calcd for $C_{21}H_{20}NO_5$ 366.1347, found

https://doi.org/10.1021/acsomega.2c05206
ACS Omega 2022, 7, 33614−33628

366.1351; $[M + H]^+$ calcd for $C_{21}H_{22}NO_5$ 368.1492, found 368.1502.

*2.2.17. N-(4-bromobenzyl)-4-hydroxy-6,8-dimethoxy-2-naphthamide (**7a**).* White solid, mp 142−143 °C. ^{1}H NMR (500 MHz, DMSO-d_6, δ ppm): 10.17 (1H, s, -OH), 9.01 (1H, s, -NH-), 8.08 (1H, d, J = 2.0 Hz, H_{Ar}), 7.86 (2H, d, J = 8.0 Hz, H_{Ar}), 7.33 (1H, d, J = 2.0 Hz, H_{Ar}), 7.17 (2H, d, J = 8.5 Hz, H_{Ar}), 7.03 (1H, d, J = 2.0 Hz, H_{Ar}), 6.65 (1H, d, J = 2.0 Hz, H_{Ar}), 4.44 (2H, d, J = 5.5 Hz, -CH_2-), 3.94 (3H, s, -OCH_3), 3.89 (3H, s, -OCH_3). ^{13}C NMR (125 MHz, DMSO-d_6, δ ppm): 166.9, 158.6, 156.7, 152.6, 136.6, 135.2, 133.3, 129.8, 128.7, 127.8, 127.2, 112.3, 107.7, 98.8, 92.6, 55.6, 55.4, 43.2. LC-MS (m/z) $[M - H]^-$ calcd for $C_{20}H_{17}BrNO_4$ 414.0346, found 414.0340; $[M + H]^+$ calcd for $C_{20}H_{19}BrNO_4$ 416.0492, found 416.0485.

*2.2.18. N-(4-bromobenzyl)-4-hydroxy-5,7-dimethoxy-2-naphthamide (**7b**).* White solid, mp 145−146 °C. ^{1}H NMR (500 MHz, DMSO-d_6, δ ppm): 10.16 (1H, s, -OH), 9.02 (1H, s, -NH-), 8.08 (1H, d, J = 2.0 Hz, H_{Ar}), 7.87 (2H, d, J = 7.0 Hz, H_{Ar}), 7.32 (1H, d, J = 2.0 Hz, H_{Ar}), 7.16 (2H, d, J = 7.0 Hz, H_{Ar}), 7.03 (1H, d, J = 2.5 Hz, H_{Ar}), 6.65 (1H, d, J = 2.0 Hz, H_{Ar}), 4.43 (2H, d, J = 5.5 Hz, -CH_2-), 3.95 (3H, s, -OCH_3), 3.90 (3H, s, -OCH_3). ^{13}C NMR (125 MHz, DMSO-d_6, δ ppm): 166.8, 158.7, 156.7, 152.1, 137.2, 135.9, 129.5, 128.8, 127.5, 127.4, 121.3, 111.6, 107.8, 98.6, 92.8, 55.8, 55.3, 42.5. LC-MS (m/z) $[M - H]^-$ calcd for $C_{20}H_{17}BrNO_4$ 414.0346, found 414.0351; $[M + H]^+$ calcd for $C_{20}H_{19}BrNO_4$ 416.0492, found 416.0497.

*2.2.19. N-(4-chlorobenzyl)-4-hydroxy-6,8-dimethoxy-2-naphthamide (**8a**).* White solid, mp 147−148 °C. ^{1}H NMR (500 MHz, DMSO-d_6, δ ppm): 10.17 (1H, s, -OH), 9.02 (1H, s, -NH-), 8.08 (1H, d, J = 1.0 Hz, H_{Ar}), 7.68 (2H, d, J = 8.0 Hz, H_{Ar}), 7.33 (1H, d, J = 2.0 Hz, H_{Ar}), 7.13 (2H, d, J = 7.5 Hz, H_{Ar}), 7.03 (1H, d, J = 2.0 Hz, H_{Ar}), 6.65 (1H, d, J = 2.0 Hz, H_{Ar}), 4.44 (2H, d, J = 6.0 Hz, -CH_2-), 3.92 (3H, s, -OCH_3), 3.90 (3H, s, -OCH_3). ^{13}C NMR (125 MHz, DMSO-d_6, δ ppm): 166.7, 158.6, 156.9, 152.4, 136.9, 135.4, 133.2, 129.7, 128.6, 127.7, 127.3, 112.2, 107.6, 98.7, 92.6, 55.6, 55.4, 43.3. LC-MS (m/z) $[M - H]^-$ calcd for $C_{20}H_{17}ClNO_4$ 370.0852, found 370.0873; $[M + H]^+$ calcd for $C_{20}H_{19}ClNO_4$ 372.0997, found 372.0976.

*2.2.20. N-(4-chlorobenzyl)-4-hydroxy-5,7-dimethoxy-2-naphthamide (**8b**).* White solid, mp 149−150 °C. ^{1}H NMR (500 MHz, DMSO-d_6, δ ppm): 10.19 (1H, s, -OH), 9.01 (1H, s, -NH-), 8.07 (1H, d, J = 2.0 Hz, H_{Ar}), 7.61 (2H, d, J = 7.5 Hz, H_{Ar}), 7.33 (1H, d, J = 2.5 Hz, H_{Ar}), 7.14 (2H, d, J = 8.0 Hz, H_{Ar}), 7.03 (1H, d, J = 2.0 Hz, H_{Ar}), 6.65 (1H, d, J = 2.0 Hz, H_{Ar}), 4.49 (2H, d, J = 5.5 Hz, -CH_2-), 3.98 (3H, s, -OCH_3), 3.84 (3H, s, -OCH_3). ^{13}C NMR (125 MHz, DMSO-d_6, δ ppm): 166.8, 158.6, 156.8, 152.0, 137.2, 135.8, 129.5, 128.6, 127.6, 127.3, 121.3, 111.7, 107.8, 98.5, 92.7, 55.8, 55.4, 42.3. LC-MS (m/z) $[M - H]^-$ calcd for $C_{20}H_{17}ClNO_4$ 370.0852, found 370.0859; $[M + H]^+$ calcd for $C_{20}H_{19}ClNO_4$ 372.0997, found 372.0990.

2.3. In Vitro Antimicrobial Activity. Antimicrobial assays were performed using a microtitre broth dilution method with ciprofloxacin (an antibacterial drug) and fluconazole (an antifungal drug) as positive controls.[1] Briefly, the test trays were incubated for 24−48 h at 37 °C for bacterial strains on nutrient agar medium and for 48 h at 25 °C for fungal strains on potato dextrose agar. The different concentration gradients of tested compounds and positive controls in the media were set to 2, 4, 8, 16, 32, 64, 128, 256, 512, and 1024 μg/mL. The inoculum was prepared by dilution in broth media of each bacterium and fungus to give a final concentration of 5×10^5 CFU/mL. The trays were then incubated at 35 °C for 18−20 h with bacteria and at 25 °C for 72 h with fungi. The MIC was determined to be the lowest concentration that completely inhibits the growth of the organism. All MIC determinations were repeated in triplicate in independent experiments.

2.4. In Vitro Anticancer Activity. The cytotoxic activity was performed using the methyl thiazolyl tetrazolium (MTT) method with paclitaxel (anticancer drug) as the positive control. The MTT assay detects the reduction of yellow tetrazolium by metabolically active cells to be purple formazan measured using spectrophotometry.[24] The tumor cell lines were grown on 96-well plates with media consisting of 10% fetal calf serum (FCS), Eagle's minimum essential medium, 2 mM L-glutamine, 100 μg/mL streptomycin, and 100 IU/mL penicillin with a density of 5×10^3 cells per well. The 96-well plates were incubated at 37 °C for 24 h in 5% CO_2. The eight concentrations of tested compounds and paclitaxel (0.5, 1, 5, 10, 25, 50, 80, and 100 μM) in DMSO were then added to each well of 96-well plates (six replicates) using the control DMSO at the same concentration and incubated for 48 h. After that, 10 μL of a fresh solution of MTT reagent was added to each well and incubated at 37 °C for 4 h in 5% CO_2. The cells were dissolved in ethanol after the purple precipitate was obtained. The optical density (OD) was measured at 570 nm using a microplate reader. The percent of proliferation inhibition was calculated using the following formula

$$\text{viability cells inhibition}(\%) = 100 - \left[\frac{(OD_t - OD_b)}{(OD_c - OD_b)}\right] \times 100\%$$

where OD_t is the optical density of the test compound, OD_b is the optical density of blank, and OD_c is the optical density of control.

The percent of proliferation inhibition versus the corresponding concentrations of the compound was plotted. The 50% inhibitory concentration (IC_{50}) of each compound was obtained using Graphpad Prism version 8.30.

2.5. In Silico ADMET Prediction. The physicochemical properties of all compounds were calculated using the SwissADME web tool. *In silico* prediction of the absorption, distribution, metabolism, and excretion (ADME) properties and the toxicity (T) risks was performed using an ADMETlab 2.0 descriptor algorithm protocol.[1,25]

2.6. Molecular Docking Studies. The structure and energy of ligands were drawn and minimized using a ChemBioDraw Ultra 19.0. The ligand molecules with minimized energy were carried out in the docking simulation using AutoDock Vina.[26,27] Protein molecules of dihydrofolate reductase (PDB ID 3GHW) and vascular endothelial growth factor receptor 2 (PDB ID 2HO4) were retrieved from the protein data bank. The receptors were added to only polar hydrogen and Kollman charges after all of the water molecules have been removed. The grid box for docking simulations was set by AutoDock tools. The ligands were docked with the target to determine the docking parameters using AutoDock Vina with the help of grid-based ligand docking. The pictorial representation of the interaction between the ligands and the target protein was performed by BIOVIA Discovery Studio 2021 software.

2.7. In Vitro Dihydrofolate Reductase Inhibition Assay. The dihydrofolate reductase (DHFR) inhibition assay was performed by the CS0340 DHFR assay kit (Sigma). Stock solutions (10 mM) of dihydrofolic acid and NADPH (reduced nicotinamide adenine dinucleotide phosphate) were prepared in assay buffer, pH 7.5. Stock solutions of the test compounds were

https://doi.org/10.1021/acsomega.2c05206
ACS Omega 2022, 7, 33614−33628

Scheme 1. Synthesis of *N*-(4-substituted benzyl) and *N*-(3-morpholinopropyl) 2-Naphthamide Derivatives[a]

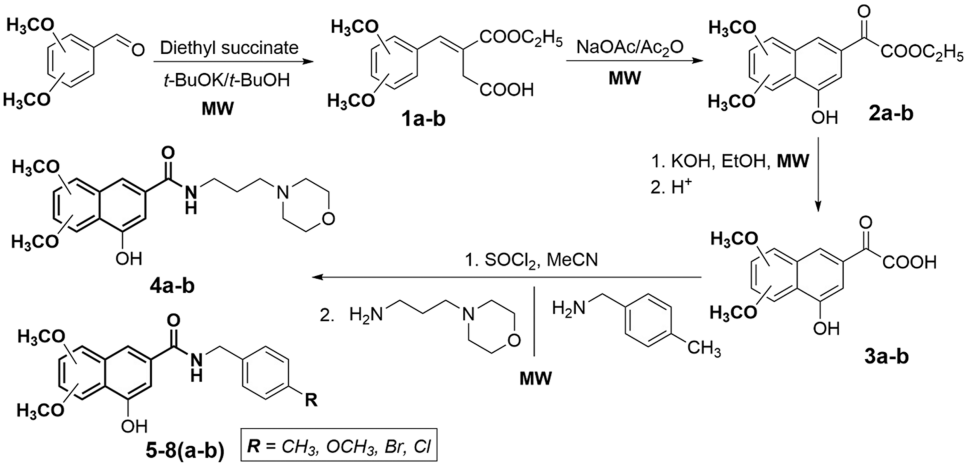

[a]MW, microwave irradiation; *t*-BuOK, potassium tert-butoxide; *t*-BuOH, *tert*-butanol; NaOAc, sodium acetate; Ac_2O, acetic anhydride; EtOH, ethanol; MeCN, acetonitrile.

Table 1. Yields and Physicochemical Parameters of *N*-(4-substituted Benzyl) and *N*-(3-morpholinopropyl) 2-Naphthamide Derivatives (4a−4b and 5a−5b)[a]

						yield	
entry	group	R	code	physicochemical parameters		Re	MW
1	6,8-$(OCH_3)_2$		**4a**	m. wt: 374.43	NRB: 8	81	93
				NHA: 6	Log *P*: 2.19		
				NHD: 2	PSA: 80.26		
2	5,7-$(OCH_3)_2$		**4b**	m. wt: 374.43	NRB: 8	82	94
				NHA: 6	Log *P*: 2.11		
				NHD: 2	PSA: 80.26		
3	6,8-$(OCH_3)_2$	-CH_3	**5a**	m. wt: 351.40	NRB: 6	82	96
				NHA: 4	Log *P*: 3.58		
				NHD: 2	PSA: 67.79		
4	5,7-$(OCH_3)_2$	-CH_3	**5b**	m. wt: 351.40	NRB: 6	83	95
				NHA: 4	Log *P*: 3.60		
				NHD: 2	PSA: 67.79		
5	6,8-$(OCH_3)_2$	-OCH_3	**6a**	m. wt: 367.40	NRB: 7	86	97
				NHA: 5	Log *P*: 3.20		
				NHD: 2	PSA: 77.02		
6	5,7-$(OCH_3)_2$	-OCH_3	**6b**	m. wt: 367.40	NRB: 7	85	97
				NHA: 5	Log *P*: 3.28		
				NHD: 2	PSA: 77.02		
7	6,8-$(OCH_3)_2$	-Br	**7a**	m. wt: 416.27	NRB: 6	80	94
				NHA: 4	Log *P*: 3.86		
				NHD: 2	PSA: 67.79		
8	5,7-$(OCH_3)_2$	-Br	**7b**	m. wt: 416.27	NRB: 6	81	95
				NHA: 4	Log *P*: 3.90		
				NHD: 2	PSA: 67.79		
9	6,8-$(OCH_3)_2$	-Cl	**8a**	m. wt: 371.81	NRB: 6	83	96
				NHA: 4	Log *P*: 3.77		
				NHD: 2	PSA: 67.79		
10	5,7-$(OCH_3)_2$	-Cl	**8b**	m. wt: 371.81	NRB: 6	84	95
				NHA: 4	Log *P*: 3.82		
				NHD: 2	PSA: 67.79		

[a]**Re** and **MW**, yields of conventional heating (or reflux) and microwave-assisted method (%); **Re**, reflux; **MW**, microwave; **M. Wt**, molecular weight; **NHA**, number of hydrogen bond acceptors; **NHD**, number of hydrogen bond donors; **NRB**, number of rotatable bonds; **PSA**, polar surface area (Angstroms squared).

prepared in DMSO and added to the mixture in different concentrations such as 10^{-8}, 10^{-7}, 10^{-6}, 10^{-5}, and 10^{-4} M in the respective wells of 96-well plates containing assay buffer. The final concentration of DMSO in each experiment was 0.4%. The changes in absorbance at 340 nm were monitored as a function of time using the test compounds and methotrexate (as a

https://doi.org/10.1021/acsomega.2c05206
ACS Omega 2022, 7, 33614−33628

Table 2. Antimicrobial Activity (MIC, μg/mL) of Synthesized Compounds 4a−4b, 5a−8a, and 5b−8b[a]

		antibacterial						antifungal	
entry	code	EC	PA	SF	SE	MSSA	MRSA	CA	AN
1	**4a**	128	128	128	64	64	256	128	256
2	**4b**	128	128	128	64	64	256	64	256
3	**5a**	64	64	64	64	32	128	128	256
4	**5b**	64	64	**32**	**32**	**16**	**32**	64	256
5	**6a**	64	64	64	64	32	128	256	256
6	**6b**	64	128	32	32	32	32	64	256
7	**7a**	64	64	64	64	32	128	128	256
8	**7b**	64	64	32	32	32	64	64	256
9	**8a**	64	64	64	64	32	128	64	256
10	**8b**	**16**	64	**16**	**16**	**8**	**16**	64	256
11	**Cipro**	16	16	8	8	8	16	ND	ND
12	**Flu**	ND	ND	ND	ND	ND	ND	4	128

[a]**ND**, not determined; **Cipro**, ciprofloxacin; **Flu**, fluconazole; **MIC** (μg/mL), ±0.5 μg/mL; **EC**, *Escherichia coli* ATCC 25922; **PA**, *Pseudomonas aeruginosa* ATCC 27853; **SF**, *Streptococcus faecalis* ATCC 29212; **SE**, *Salmonella enterica* ATCC 10428; **MSSA**, methicillin-susceptible strains of *Staphylococcus aureus* ATCC 29213; **MRSA**, methicillin-resistant strains of Staphylococcus aureus ATCC 43300; **CA**, *Candida albicans* ATCC 10321; **AN**, *Aspergillus niger* ATCC 16404. The values in bold highlight the best compounds with the best MIC values compared to positive controls.

positive control). Percentage inhibition of enzymatic activity was calculated after nullifying the effects of NADPH, folate, and solvent. The 50% inhibitory concentration (IC_{50}) of each compound was calculated by plotting a graph between percentage inhibition and the corresponding concentration of the compound using Graphpad Prism version 8.30.

2.8. In Vitro VEGFR-2 Inhibition Assay. The VEGFR-2 tyrosine kinase activity was tested using the VEGFR-2 kinase assay kit (BPS-Bioscience). In brief, the different dilutions (10^{-8}, 10^{-7}, 10^{-6}, 10^{-5}, and 10^{-4} M) of the VEGFR-2 enzyme and tested compounds were added to the wells of a 96-well plate and incubated at 30 °C for 30 min. Next, 25 mL of ADP-GloTM reagent was added and incubated at room temperature for 45 min. Finally, the kinase detection reagent (Kinase-Glo MAX, Promega) was added to each well. A luminescence signal was detected and quantified by a microplate reader for the determination of the IC_{50} value of tested compounds after subtracting the blank control value.

2.9. Statistical Analysis. All values are expressed in mean ± SEM (standard error of the mean). The differences in IC_{50} value between tested compounds and paclitaxel were analyzed by one-way ANOVA with Tukey's HSD post-hoc test using Minitab 19.0 software. The p-value < 0.05 indicates statistically significant.

3. RESULTS AND DISCUSSION

3.1. Chemistry. 2,4-Dimethoxybenzaldehyde and 3,5-dimethoxybenzaldehyde are the starting materials for the preparation of *N*-(4-substituted benzyl) and *N*-(3-morpholinopropyl) 2-naphthamide derivatives. The synthesis of the compounds consists of four steps (Scheme 1). The Stobbe condensation was carried out with diethyl succinate using potassium *tert*-butoxide and *tert*-butanol by a microwave-assisted method to yield two (dimethoxyphenyl)-3-(ethoxycarbonyl)but-3-enoic acid derivatives (**1a−1b**). In the second step, cyclization was carried out with sodium acetate and acetic anhydride agents to form 2-naphthoate derivatives (**2a−2b**) by the microwave-assisted method with excellent yields (91−93%). Next, the ester hydrolysis was carried out in an alkaline environment to yield naphthalene-2-carboxylic acid derivatives (**3a−3b**). Finally, two carboxylic acid derivatives were converted to acyl halide derivatives with thionyl chloride, followed by an amidation reaction to yield *N*-(4-substituted benzyl) and *N*-(3-morpholinopropyl) 2-naphthamide derivatives (**4a−4b**, **5a−8a**, and **5b−8b**). In the final stage, the reaction time has been dramatically reduced, as using conventional heating, the reaction is carried out in 3.5 h compared with 30 min heating in the microwave. In addition, the reaction yield has increased ranging between 12 and 13% with microwave assistance (Table 1). All compounds have physical−chemical properties of fragments (M. Wt < 500) that follow Lipinski's rules, which can lead to potent compounds for further development,[23] especially 10 derivatives (**4−8**) are new compounds.

^{1}H NMR, ^{13}C NMR, and mass spectra of the synthesized compounds are in accordance with the assigned structures. The ^{1}H NMR spectra of compounds **4−8** indicated the characteristic NH protons of the amide group as a singlet in the δ 9.04−8.52 ppm region as well as the distinctive aromatic protons in the δ 8.09−6.63 ppm region. On the other hand, ^{1}H NMR spectra of compounds **4−8** revealed the appearance of a singlet in the 3.99−3.84 ppm region of the methoxy (-OCH_3) moiety. In addition, ^{1}H NMR spectra revealed the appearance of the 3-morpholinopropyl group of compound **4** in the 3.59−1.67 ppm region as well as the methylene (-CH_2-Ar) group in the 4.49−4.33 ppm region and the methyl (-CH_3) group in the 2.29−2.27 ppm region of compound **5**. Furthermore, the C═O moiety of the amide group (δ 167.0−166.6 ppm), C_{Ar} (δ 159.0−92.6 ppm), methoxy group (δ 56.0−55.2 ppm), the methylene moiety of the benzyl group (δ 43.3−42.1 ppm), C_{alkyl} of the 3-morpholinopropyl group (δ 66.3−38.2 ppm), and the methyl group (δ 25.8−25.7 ppm) were identified in the ^{13}C NMR spectrum of compounds **4−8**. The molecular ion peak M (m/z) of compounds **4−8** was observed in the mass spectrum, confirming the hypothesized structure.

3.2. In Vitro Antimicrobial Activities. Antimicrobial activities (exhibited by MIC values) including antifungal activities (CA, *Candida albicans* and AN, *Aspergillus niger*) and antibacterial activities against three Gram-negative strains (EC, *Escherichia coli*; PA, *Pseudomonas aeruginosa*; *SE—Salmonella enterica*) and three of Gram-positive strains (SF—*Streptococcus*

https://doi.org/10.1021/acsomega.2c05206
ACS Omega 2022, 7, 33614−33628

faecalis, MSSA, MRSA) of all synthesized compounds are summarized in Table 2.

Compounds **4a**, **4b**, **6a**−**8a**, and **6b**−**7b** showed weak to moderate activities against six strains of bacteria (EC, PA, SF, SE, MSSA, and MRSA) and two strains of fungi (CA and AN) with MIC ≥ 32 μg/mL. Compound **5b** (5,7-dimethoxy, *N*-(4-methylbenzyl)) showed good antibacterial activities against one Gram-negative strain SE and three Gram-positive strains SF, MSSA, and MRSA with MIC ranging between 16 and 32 μg/mL as compared to ciprofloxacin (Cipro, MIC = 8−16 μg/mL) but showed moderate activities against the bacterial strains EC and PA with MIC of 64 μg/mL. Moreover, compound **8b** (5,7-dimethoxy, *N*-(4-chlorobenzyl)) showed potent antibacterial activities against all tested Gram-negative (EC and SE) and Gram-positive (SF, MSSA, and MRSA) strains, except for the PA strain with MIC ranging between 8 and 16 μg/mL as compared to ciprofloxacin. In addition, compounds **5b** and **8b** showed moderate activities against two fungi strains CA and AN with MIC of 64 and 256 μg/mL, respectively, as compared to Flu (MIC of 4 μg/mL at CA and 128 μg/mL at AN). From the structure−activity relationship (SAR), the presence of the 5,7-dimethoxy groups in the naphthalene ring and the *N*-(4-methylbenzyl)/ *N*-(4-chlorobenzyl) group is more desirable for enhanced antibacterial activities against SE, SF, MSSA, and MRSA strains in **5b** and **8b**.

In published studies, *N*-(-4-aryloxyphenyl) 1-naphthamide derivatives exhibited potent antibacterial and antifungal activities against Gram-positive bacteria *Staphylococcus aureus* and Gram-negative bacteria *Escherichia coli* and two pathogenic fungal strains *Aspergillus niger* and *Candida albicans* with the zone of inhibition in (mm) equivalent to that of the reference standard drugs ciprofloxacin and voriconazole.[15] In addition, *N*-pyridin-4-ylmethyl alkyl-2-naphthamide and phenylpropan-2-yl alkyl-2-naphthamide derivatives showed excellent broad-spectrum antifungal properties (including *Candida albicans*, *Candida glabrata*, *Candida krusei*, and *Candida tropicalis*) with MIC_{50} ranging between 0.125 and 0.250 μg/mL comparable to fluconazole and naftifine (MIC_{50} = 0.25−2.00 μg/mL) and also exhibited the obvious antifungal effects against drug-resistant fungi with MIC_{50} ranging between 2 and 8 μg/mL comparable to fluconazole (MIC_{50} > 16 μg/mL) and naftifine (MIC_{50} = 8 to >16 μg/mL).[17] Moreover, *N*-(4-phenylpiperazin-1-y)/*N*-cyclohexyl/*N*-(2-trifluoromethylphenyl) 4-alkoxy-2-naphthamide derivatives were able to synergize with the antibiotics tested and inhibit Nile Red efflux by AcrB in the resistant phenotype as well as displayed a significant increase in efficacy as efflux pump inhibitors against the *Escherichia coli* strain BW25113.[14] Similar to reported potent compounds in the literature, our active 2-naphthamide derivatives (**5b** and **8b**) contain the 4-hydroxy group on the naphthalene ring and the *N*-arylmethyl group of the 2-naphthamide nucleus. Compound **8b** also showed good antibacterial activity against *Escherichia coli* with the MIC value of 16 μg/mL similar to *N*-(-4-aryloxyphenyl) 1-naphthamide and 4-alkoxy-2-naphthamide derivatives.[14,15] Besides, compound **8b** (*N*-(4-chlorobenzyl)) exhibited more than 2-fold potential antibacterial activity against bacterial strains SF, SE, MSSA, and MRSA than compound **5b** (*N*-(4-methylbenzyl)). This may be due to the different four-substituted moieties of the *N*-benzyl group (Figure 3).

3.3. Anticancer Activity. The potent anticancer activity of synthesized compounds was tested against four cancer cell lines (C26, colon carcinoma cell line; HepG2, hepatocellular carcinoma cell line; MCF7, human breast cancer cell line; and

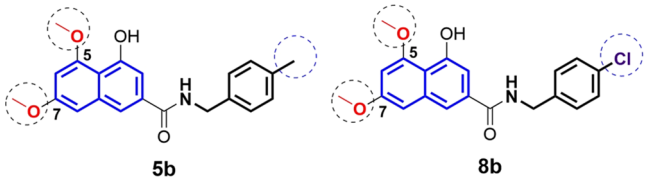

Figure 3. Structure of potentially anticancer active compounds **5b** and **8b**.

H69PR, human small cell lung cancer cell line) using paclitaxel (PTX) as a nonselective positive control. The results are summarized in Table 3.

Compounds **4a**−**8a** and **4b**−**7b** exhibited weak activity (IC_{50} = 21.29−53.68 μM) against the H69PR cell line, but only compound **8b** (5,7-dimethoxy, *N*-(4-chlorobenzyl)) showed good anticancer activity against the H69PR cell line with an IC_{50} value of 12.79 μM as compared to PTX (IC_{50} = 7.29 μM). In addition, compounds **4a**, **4b**, **6a**, and **7a** exhibited moderate activity (IC_{50} = 14.47−25.05 μM) against C26, HepG2, and MCF7 cell lines. Compounds **5a** (6,8-dimethoxy, *N*-(4-methylbenzyl)), **6b** (5,7-dimethoxy, *N*-(4-methoxybenzyl)), **7b** (5,7-dimethoxy, *N*-(4-bromobenzyl)), and **8a** (6,8-dimethoxy, *N*-(4-chlorobenzyl)) showed moderate activity (IC_{50} = 10.34−13.34 μM) against the MCF7 cell line with IC_{50} values less potential than PTX (IC_{50} = 2.85 μM) about 3.83 to 4.68 times but exhibited good anticancer activity against C26 (IC_{50} = 8.61−12.33 μM) and HepG2 (IC_{50} = 10.08−13.96 μM) cell lines with IC_{50} values larger than PTX (IC_{50} = 3.96−5.75 μM) about 1.75−2.43 times. Moreover, compound **5b** (5,7-dimethoxy, *N*-(4-methylbenzyl)) showed potent anticancer activity against C26, HepG2, and MCF7 with IC_{50} of 3.59, 8.38, and 6.75 μM, respectively, as compared to PTX. However, compound **5b** exhibited weak anticancer activity against H69PR with the IC_{50} of 28.45 μM. In particular, compound **8b** showed the strongest anticancer activity among all compounds against C26, HepG2, and MCF7 with IC_{50} of 2.97, 7.12, and 3.58 μM, respectively, as compared to PTX. As seen in Figure 4, compounds **5b** and **8b** exhibited better anticancer activity than PTX on the C26 cell line but exhibited weaker anticancer activity than PTX on HepG2, MCF7, and H69PR cell lines. Target engagement with electron-donating substituent -OCH_3 at positions 5 and 7 on the naphthalene ring and the *N*-(4-methylbenzyl)/*N*-(4-chlorobenzyl) group may be responsible for its anticancer activity as compared to other compounds.

In published studies with similar structures, one chalcone containing a naphthalene moiety with a diethylamino group at the para position of the phenyl ring showed potent anticancer activity against HCT116 and HepG2 cell lines with IC_{50} values of 1.20 and 1.02 μM, respectively.[11] Moreover, 6-aryloxy *N*-methyl 1-naphthamide exhibited selective and equally high potency against FGFR1/2 and VEGFR-2 with IC_{50} values less than 5.0 nM.[10] In particular, the anilinopyrimidine-based 1-naphthamide derivative with the *N*-phenyl group showed high VEGFR-2 inhibitory potency in both enzymatic and VEGF-induced HUVEC (human umbilical vein endothelial cell) proliferation assays with IC_{50} values of 0.5 and 9.8 nM, respectively.[12] Similar to reported potent compounds in the literature, our active 2-naphthamide derivatives (**5b** and **8b**) contain the *N*-alkyl or *N*-arylmethyl group (Figure 3). Besides, compounds **5b**−**8b** (5,7-dimethoxy) exhibited better anticancer activity than compounds **5a**−**8a** (6,8-dimethoxy) against C26, HepG2, and MCF7 cancer cell lines. This result has shown that

https://doi.org/10.1021/acsomega.2c05206
ACS Omega 2022, 7, 33614−33628

Table 3. Anticancer Activity (IC_{50}, μM) of Synthesized Compounds 4a−4b, 5a−8a, and 5b−8b[a]

		anticancer			
entry	code	C26	HepG2	MCF7	H69PR
1	**4a**	23.84 ± 2.93	14.47 ± 2.02	16.09 ± 2.42	52.24 ± 4.81
2	**4b**	25.05 ± 3.23	17.82 ± 2.46	18.56 ± 1.84	53.68 ± 3.55
3	**5a**	9.21 ± 2.30	13.61 ± 1.37	10.34 ± 2.11	34.18 ± 5.64
4	**5b**	**3.59 ± 1.04**	**8.38 ± 1.14**	**6.75 ± 1.95**	**28.45 ± 3.70**
5	**6a**	14.38 ± 1.62	17.40 ± 1.51	15.91 ± 1.28	29.24 ± 2.65
6	**6b**	12.33 ± 2.15	13.96 ± 1.40	13.34 ± 2.69	28.49 ± 3.29
7	**7a**	18.50 ± 1.73	16.72 ± 1.68	19.82 ± 1.59	22.98 ± 2.87
8	**7b**	9.83 ± 1.54	12.05 ± 1.09	11.45 ± 1.61	21.29 ± 3.04
9	**8a**	8.61 ± 1.49	10.08 ± 1.17	12.36 ± 1.34	25.45 ± 3.02
10	**8b**	**2.97 ± 0.98**	**7.12 ± 1.25**	**3.58 ± 1.06**	**12.79 ± 2.83**
11	**PTX**	3.96 ± 0.54	5.75 ± 0.60	2.85 ± 0.43	7.29 ± 0.91

[a]IC_{50} ± SEM (μM, SEM—standard error of the mean); **PTX**, paclitaxel; **C26**, colon carcinoma cell line; **HepG2**, human hepatocyte carcinoma cell line; **MCF7**, human breast cancer cell line; **H69PR**, human small cell lung cancer cell line. The values in bold highlight the best compounds with the best IC_{50} values compared to positive controls.

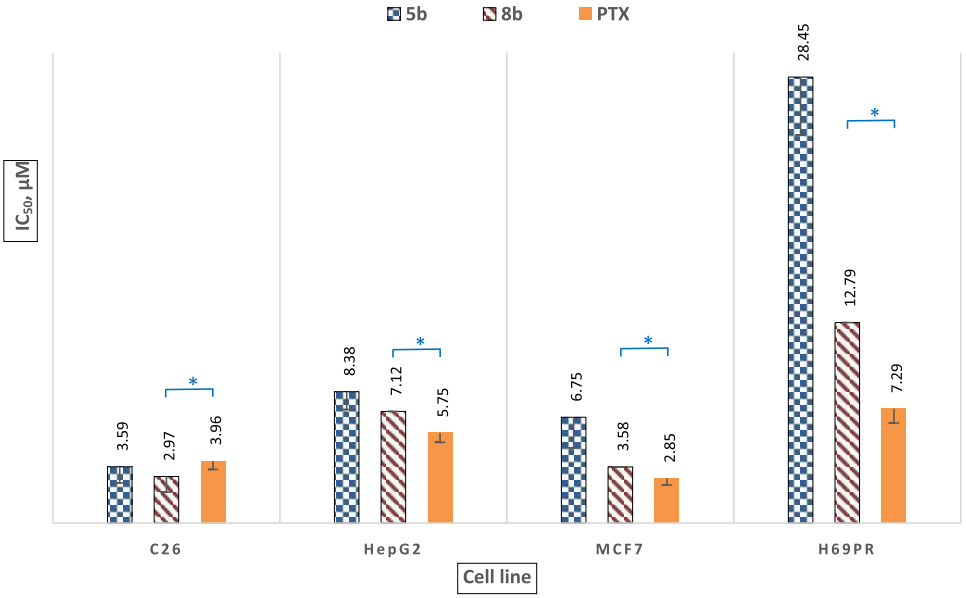

Figure 4. Comparison of anticancer activity (IC_{50} values) between active compounds and PTX (C26, colon carcinoma cell line; HepG2, human hepatocyte carcinoma cell line; MCF7, human breast cancer cell line; H69PR, human small cell lung cancer cell line; PTX, paclitaxel; (*), significantly different compared with IC_{50} of 8b and PTX with $p < 0.05$).

the positions of two methoxy groups on the naphthalene nucleus have an important role in enhancing the antitumor activity.

3.4. In Silico ADMET Profile. In the present study, a computational study of the two most active compounds was conducted to determine the surface area and other physicochemical properties, according to the directions of Lipinski's rule.[24] Lipinski suggested that the absorption capacity of a compound is much better if the molecule achieves at least three out of four of the following rules: (i) HB donor groups ≤ 5, (ii) HB acceptor groups ≤ 10, (iii) M. Wt less than 500, and (iv) log *P* less than 5. In this study, compounds **5a** and **5b** follow all Lipinski's rules. All of the highest active derivatives have a number of hydrogen bonding acceptor groups ranging between 4 and 6 and hydrogen bonding donor groups of 2. Also, molecular weights range from 351.50 to 374.43 and log *P* values range between 2.12 and 2.89, and all of these values agree with Lipinski's rules.

After assessing ADMET profiles of active compounds (Table 4), we can suggest that these derivatives have the advantage of better intestinal absorption in humans than Cipro, Flu, and PTX, as all compounds showed Caco-2 permeability higher than the control drugs and higher than −5.15 log unit. Besides, compounds **5b** and **8b** showed high passive MDCK permeability (>20 × 10^{-6} cm/s) as compared to the reference drugs. In addition, all compounds showed good plasma protein binding capacity with PPB > 98.0% as compared to Cipro (PPB = 37%), Flu (PPB = 62%), and PTX (95%). As for prediction of the BBB (blood−brain barrier) permeability, compounds **5b** and **8b** demonstrated the inability to penetrate BBB similar to Cipro and PTX. Therefore, toxicity and side effects on the brain as well as the central nervous system may not appear.

Two active compounds **5b** (log Kp of −5.67 cm/s) and **8b** (log Kp of −5.61 cm/s) showed better skin permeation than Cipro (log Kp of −9.09 cm/s) and Flu (log Kp of −7.92 cm/s). The cytochrome enzymes could be moderate to strongly inhibited under the effect of active compounds especially CYP1A2 and CYP2D6, while Cipro and Flu could not. These compounds also showed the effect of CYP2C9 and CYP3A4

https://doi.org/10.1021/acsomega.2c05206
ACS Omega 2022, 7, 33614−33628

Table 4. ADMET Profile of the Most Active Compounds Ciprofloxacin, Fluconazole, and Paclitaxel[a,ab]

parameter	5b	8b	Cipro	Flu	PTX
		Absorption			
Caco-2 permeability	−4.946	−4.955	−5.269	−4.950	−5.461
MDCK permeability	1.2×10^{-5}	1.5×10^{-5}	3.0×10^{-6}	2.8×10^{-5}	5.4×10^{-5}
Pgp-inhibitor	++	−	−−−	−−−	+++
Pgp-substrate	−−−	−−−	+++	−−−	+++
HIA	+++	+++	+++	+++	+++
$F_{20\%}$	+++	+++	+++	+++	−−−
$F_{30\%}$	−−	++	+++	+++	−−−
		Distribution			
PPB (%)	98.627	99.350	37.456	61.763	94.571
VD (L/kg)	0.665	0.678	2.324	0.835	0.907
BBB penetration	−−	−−−	−−−	+++	−−
Fu (%)	1.631	1.067	78.856	51.002	6.779
Log Kp (cm/s)	−5.67	−5.61	−9.090	−7.920	
		Metabolism			
CYP1A2 inhibitor	++	+++	−−	-	−−−
CYP1A2 substrate	+++	+++	−−	-	−−−
CYP2C19 inhibitor	++	+++	−−−	+	−−−
CYP2C19 substrate	-	−−	−−	−−−	−−−
CYP2C9 inhibitor	++	++	−−−	−−	++
CYP2C9 substrate	++	++	−−−	+	−−−
CYP2D6 inhibitor	+	++	−−−	−	−−−
CYP2D6 substrate	++	++	−−	−−	−−−
CYP3A4 inhibitor	++	++	−−−	−	++
CYP3A4 substrate	−	−−	−−	−−	+
		Excretion			
CL (mL/min/kg)	7.876	7.201	3.214	5.960	3.416
$T_{1/2}$	0.504	0.358	0.056	0.228	0.028
		Toxicity			
hERG blockers	+	++	−−	−−−	−−
H-HT	−−	−−	+++	+++	+++
DILI	−	+	+++	+++	+++
AMES toxicity	−	−	−−	++	−−−
rat oral acute toxicity	−−−	−−−	−−	+++	−
FDAMDD	+	++	++	++	++
skin sensitization	+	+	+	+++	−−−
carcinogenicity	−−−	−−−	−	+++	−−−
eye corrosion	−−−	−−−	−−−	−−−	−−−
eye irritation	−−−	−−−	−−−	−−	−−−
respiratory toxicity	−−−	−−−	++	++	+++
		Tox21 Pathway			
NR-AR	−−−	−−−	++	−−−	−−
NR-AR-LBD	−−−	−−−	−−−	−−−	+++
NR-AhR	+++	+++	−−	+	−−−
NR-Aromatase	−−−	−−	−−−	+++	++
NR-ER	−−	−−	−	−−−	+
NR-ER-LBD	−−−	−−−	−−−	−−−	+
NR-PPAR-γ	++	++	−−−	−−−	+++
SR-ARE	+	++	−	−−	++
SR-ATAD5	+	+	−−−	−−−	+++
SR-HSE	−−	−−	−−−	−−−	−
SR-MMP	+	++	−−−	−−	+++
SR-p53	+	++	−−−	−−−	+++
		Toxicophore Rules			
acute toxicity rule	0 alert	0 alert	1 alert	0 alert	0 alert
genotoxic carcinogenicity rule	1 alert	1 alert	1 alert	0 alert	1 alert
nongenotoxic carcinogenicity rule	0 alert	1 alert	1 alert	0 alert	0 alert
skin sensitization rule	2 alerts	2 alerts	0 alert	0 alert	6 alerts
aquatic toxicity rule	0 alert	1 alert	1 alert	1 alert	2 alerts
nonbiodegradable rule	0 alert	1 alert	2 alerts	1 alert	2 alerts
SureChEMBL rule	0 alert	0 alert	0 alert	0 alert	0 alert

https://doi.org/10.1021/acsomega.2c05206
ACS Omega 2022, 7, 33614−33628

Table 4. continued

parameter	5b	8b	Cipro	Flu	PTX
FAF-Drugs4 rule	1 alert	1 alert	1 alert	1 alert	1 alert

[a]**Cipro**—ciprofloxacin, **Flu**—fluconazole, **PTX**—paclitaxel, **Caco-2 permeability** (optimal: higher than −5.15 Log unit), **MDCK permeability** (low permeability: $<2 \times 10^{-6}$ cm/s, medium permeability: $2-20 \times 10^{-6}$ cm/s, high passive permeability: $>20 \times 10^{-6}$ cm/s), **Pgp**—P-glycoprotein, **HIA**—human intestinal absorption (−: <30%, +: ≥30%), **F**—bioavailability (−: <percent value, +: ≥percent value), **PPB**—plasma protein binding (optimal: <90%), **VD**—volume distribution (optimal: 0.04−20 L/kg), **BBB**—blood-brain barrier, **Fu**—the fraction unbound in plasms (low: <5%, middle: 5−20%, high:>20%), **Log Kp** (skin permeation), **CL**—clearance (low: <5 mL/min/kg, moderate: 5−15 mL/min/kg, high:>15 mL/min/kg), $\mathbf{T_{1/2}}$ (category 1: long half-life (>3 h), category 0: short half-life (<3 h)), **H-HT**—human hepatotoxicity, **DILI**—drug-induced liver injury, **FDAMDD**—maximum recommended daily dose, **AR**—androgen receptor, **AR-LBD**—androgen receptor ligand-binding domain, **AhR**—aryl hydrocarbon receptor, **ER**—estrogen receptor, **ER-LBD**—estrogen receptor ligand-binding domain, **PPAR-γ**—peroxisome proliferator-activated receptor γ, **ARE**—antioxidant response element, **ATAD5**—ATPase family AAA domain-containing protein 5, **HSE**—heat shock factor response element, **MMP**—mitochondrial membrane potential. [b]The output value is the probability of being inhibitor/substrate/active/positive/high toxicity/sensitizer/carcinogens/corrosives/irritants (category 1) or noninhibitor/nonsubstrate/inactive/negative/low toxicity/nonsensitizer/noncarcinogens/noncorrosives/nonirritants (category 0). For the classification endpoints, the prediction probability values are transformed into six symbols: 0−0.1(−−−), 0.1−0.3(−−), 0.3−0.5(−), 0.5−0.7(+), 0.7−0.9(++), and 0.9−1.0(+++).

Table 5. *In Silico* Molecular Docking Results of Active Compounds and Standard Drugs[a]

receptor	compound	affinity (Kcal/mol)	hydrogen bond number	interaction types
DHFR	**5b**	−9.9	2	Hydrogen (ASP21 - 2.86 Å); C-Hydrogen (GLY17 - 3.49 Å); π−π (PHE34); alkyl (ILE60, LEU67, LYS55); π-alkyl (ILE16, ILE60, PHE34, VAL115)
	8b	−9.8	1	C-Hydrogen (GLU30 - 3.46 Å); π−π (PHE31, PHE34); alkyl (ALA9, PRO61, VAL8, ILE7); π-alkyl (PHE31, PHE34, ALA9, PRO61)
	PTX	−9.9	4	Hydrogen (GLY117 - 2.65 Å; THR56 - 2.09; 2.39 Å); C-Hydrogen (SER119 - 2.97 Å); π-cation (LYS55); π-alkyl (ILE16, LYS55)
VEGFR-2	**5b**	−9.5	3	Hydrogen (LEU838 - 2.03 Å; CYS917 - 1.92 Å); C-Hydrogen (GLU915 - 3.79 Å); π-σ (LEU838); π-Sulfur (CYS1043); π−π (PHE1045); alkyl (LYS866, VAL846); π-alkyl (ALA864, LEU838, VAL846, VAL914)
	8b	−9.8	1	C-Hydrogen (LYS918 - 3.73 Å); π-σ (LEU838); π−π (PHE1045); alkyl (LEU887, VAL897, CYS1043); π-alkyl (PHE916, VAL897, VAL914, CYS1043)
	PTX	−8.2	8	Hydrogen (ARG1049 - 2.68; 2.98 Å; ASN921 - 2.78 Å; LEU838 - 2.30 Å; LYS1053 - 2.39; 2.60 Å); C-Hydrogen (ASP1062 - 3.21 Å; GLY920 - 3.46 Å); π-σ (LEU838); π−π (PHE916); π-alkyl (ALA864, VAL846, VAL914)

[a]DHFR, dihydrofolate reductase; VEGFR-2, vascular endothelial growth factor receptor 2; PTX, paclitaxel.

inhibition as compared with PTX. Moreover, compounds **5b** (7.876 mL/min/kg) and **8b** (7.201 mL/min/kg) were classified as a moderate clearance level ranging between 5 and 15 mL/min/kg as compared with Flu (CL = 5.69 mL/min/kg). On the other hand, two new ligands did not show rat oral acute toxicity, carcinogenicity, eye corrosion, eye irritation, and respiratory toxicity. Therefore, these potent compounds showed lower overall toxicity than the reference drugs Cipro, Flu, and PTX. Finally, these compounds also exhibited good "Tox21 pathway" and "toxicophore rules" profiles as compared to the reference drug PTX.

3.5. In Silico Molecular Docking Studies. After ADMET profiling, docking studies were carried out to predict the most suitable binding pose and inhibition mechanism of the most active compounds. Based on the principle that similar compounds tend to bind to the same proteins as well as *in vitro* enzyme inhibition of the reported homologous naphthamide structures, two target proteins were selected, including dihydrofolate reductase (DHFR) for antibacterial and anticancer activities and vascular endothelial growth factor receptor 2 (VEGFR-2) for anticancer activity.[12,23] The protein−ligand complex is formed through hydrogen bonds (both from side chains and backbones), electrostatic interactions (π−cation and π−anion), and hydrophobic interactions (π−σ, π−π, alkyl, π−alkyl) of the binding interface (Table 5).[24]

On the DHFR receptor, compounds **5b** (−9.9 Kcal/mol) and **8b** (−9.8 Kcal/mol) showed similar high affinity for PTX (−9.9 Kcal/mol) at the active site. Compound **5b** established a conventional hydrogen bond (2.86 Å) with ASP21 amino acid and one carbon−hydrogen bond with GLY17 amino acid at the 4-hydroxy (4-OH) group with a bond length of 3.49 Å. Compound **5b** also showed hydrophobic interactions (π−π stacking, alkyl, π−alkyl) with PHE34, ILE60, LEU67, LYS55, ILE16, and VAL115 amino acids at the aromatic rings and the methyl ($-CH_3$) group with bond lengths of 3.94, 3.94, 4.63, 4.71, 4.63, and 5.26 Å, respectively. Hydrophobic interaction with LYS55 and ILE16 amino acids of compound **5b** is similar to that of PTX. Besides, compound **8b** established one carbon−hydrogen bond (3.46 Å) with GLU30 amino acid and the 7-methoxy ($7-OCH_3$) group. Similarly, compound **8b** also showed hydrophobic interactions (π−π stacking, alkyl, π−alkyl) with PHE31, PHE34, ALA9, PRO61, VAL8, and ILE7 amino acids at the aromatic rings and 4-chloro (4-Cl) group with bond lengths of 3.74, 3.97, 4.11, 4.91, 5.42, and 4.36 Å, respectively (Figure 5). These results suggested that DHFR is the most likely target for the anticancer activity of compounds **5b** and **8b**.

On the VEGFR-2 receptor, compounds **5b** and **8b** showed strong interactions with the affinities of −9.5 and −9.8 Kcal/mol, respectively, compared with the reference drug PTX (−8.2 Kcal/mol). Compound **5b** established two conventional hydrogen bonds (1.92−2.03 Å) with LEU838 and CYS917 amino acids at the 4-hydroxy (4-OH) and amide (-CONH-) groups and one carbon−hydrogen bond with GLU915 amino acid at the methylene ($-CH_2-$) moiety of the *N*-(4-methylbenzyl) group with a bond length of 3.79 Å. In addition, compound **5b** showed hydrophobic interactions (π−σ, π−sulfur, π−π, alkyl, π−alkyl) with LEU838, CYS1043, PHE1045, LYS866, VAL846, ALA864, and VAL914 amino acids with bond

https://doi.org/10.1021/acsomega.2c05206
ACS Omega 2022, 7, 33614−33628

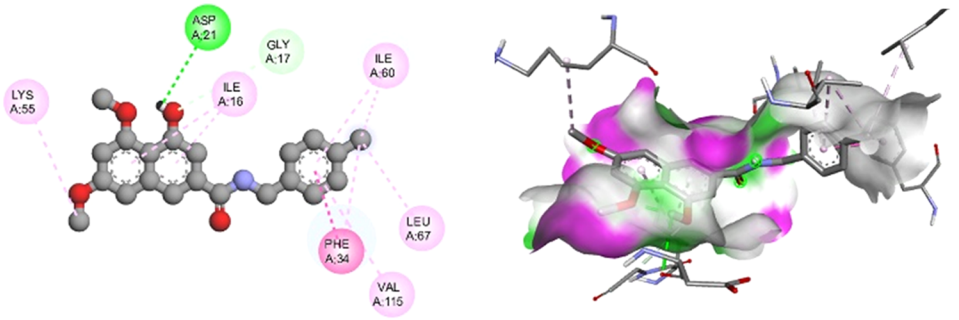

5b - DHFR

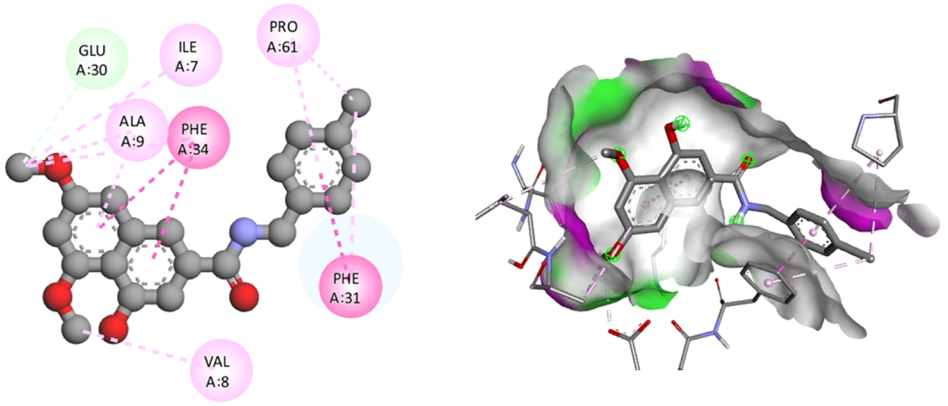

8b - DHFR

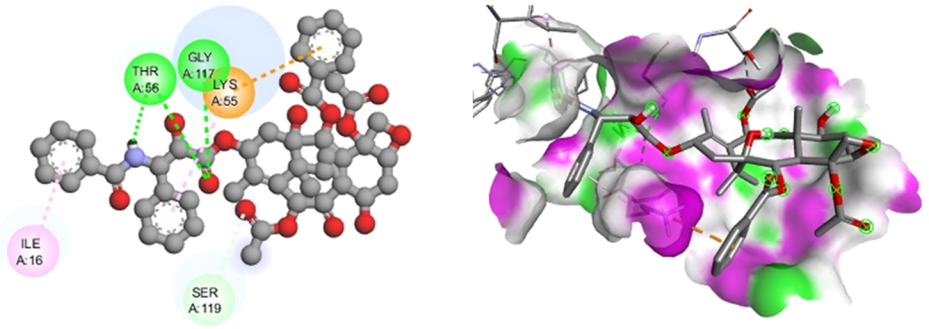

PTX - DHFR

Figure 5. 2D and 3D representation of the interaction of active molecules **5b** and **8b** and paclitaxel (PTX) with dihydrofolate reductase (DHFR).

lengths of 3.93, 5.32, 4.77, 4.35, 4.77, 5.02, and 4.88 Å, respectively (Figure 6). On the other hand, compound **8b** established one carbon-−hydrogen bond (3.46 Å) with LYS918 amino acid and the 5-methoxy (5-OCH_3) group. Compound **8b** also showed hydrophobic interactions ($\pi-\sigma$, $\pi-\pi$ T-shaped, alkyl, π−alkyl) with LEU838, PHE1045, LEU887, VAL897, CYS1043, PHE916, and VAL914 amino acids at the benzene and naphthalene rings and 4-chloro (4-Cl) group with bond lengths of 3.97, 5.37, 5.13, 3.53, 4.60, 4.98, and 4.83 Å, respectively. In particular, compounds **5b** and **8b** showed interactions with LEU838 and VAL914 with the crucial residue of the VEGFR-2 protein from *Escherichia coli* that resembles the cocrystallization ligand and PTX.

In summary, from the *in silico* molecular docking study results, it can be concluded that compounds **5b** and **8b** were considered the best dock ligand in antitumor targets such as DHFR and VEGFR-2. Moreover, compound **8b** showed a higher affinity than compound **5b** on the VEGFR-2 receptor. This may explain the result that compound **8b** showed better *in vitro* antitumor activity than compound **5b**.

3.6. In Vitro DHFR and VEGFR-2 Inhibitory Activities.

The results of *in silico* molecular docking studies have predicted

https://doi.org/10.1021/acsomega.2c05206
ACS Omega 2022, 7, 33614−33628

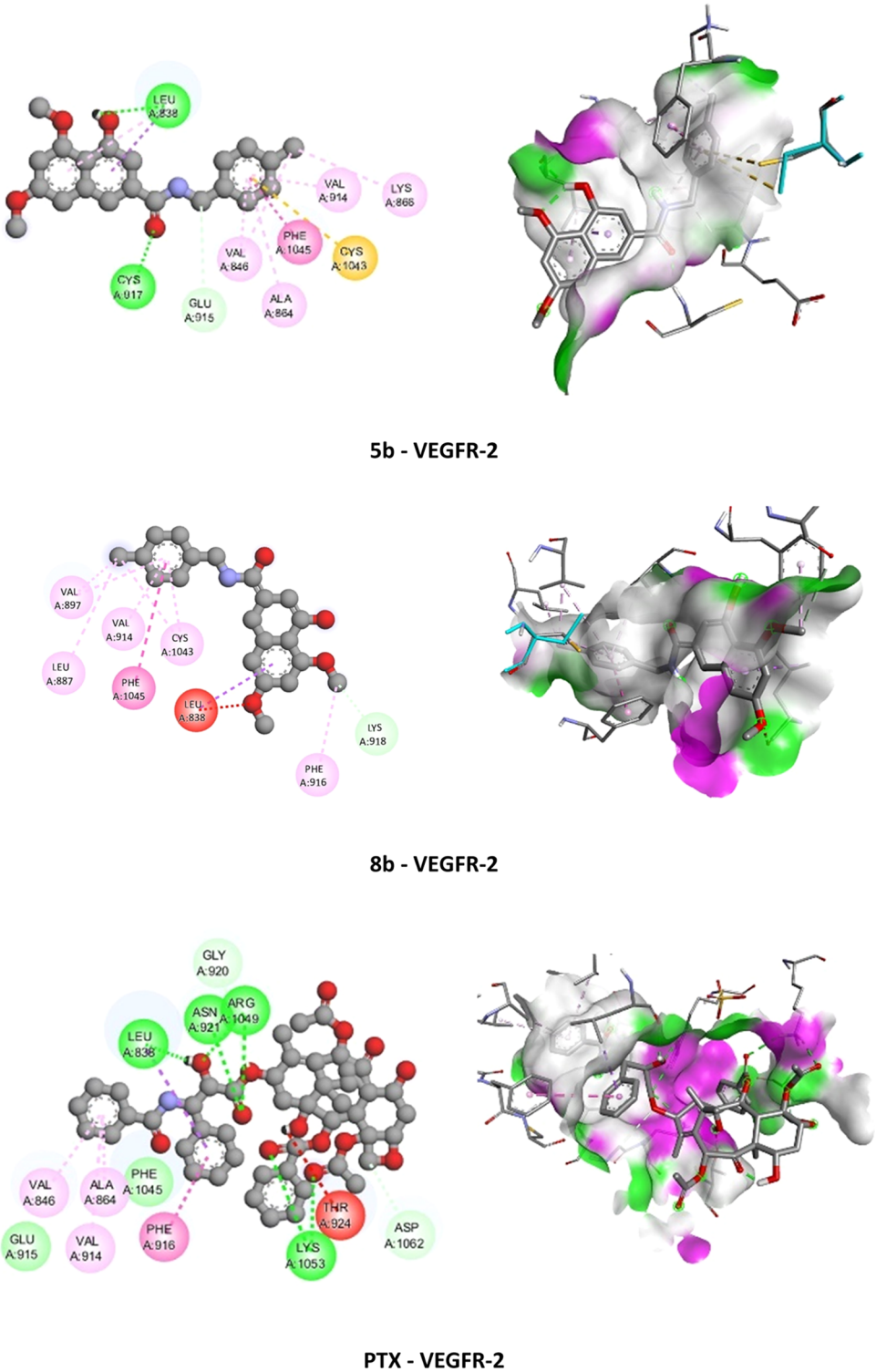

Figure 6. 2D and 3D representation of the interaction of active molecules **5b** and **8b** and paclitaxel (PTX) with vascular endothelial growth factor receptor 2 (VEGFR-2).

that DHFR and VEGFR-2 are potential receptors to explain the mechanism of antibacterial and anticancer activities for the active derivatives. Therefore, compounds **5b** and **8b** were subjected to further assay for their ability to inhibit DHFR and VEGFR-2 using methotrexate and sorafenib as positive controls. The results presented in Table 6 show that compounds **5b** and **8b** managed to inhibit DHFR kinase with IC_{50} < 10 μM and VEGFR-2 kinase with IC_{50} < 1 μM. Compounds **5b** and **8b** showed good DHFR inhibitory activity with IC_{50} values of 9.085 and 7.881 μM, respectively, compared with positive control methotrexate (IC_{50} = 0.022 μM). Especially, it has been observed that compounds **5b** and **8b** showed excellent VEGFR-2 inhibitory activity with IC_{50} values of 0.623 and 0.384 μM, respectively, which is comparable to sorafenib with the IC_{50} value of 0.069 μM. In addition, these compounds exhibited 15−20 times better inhibitory activity on the VEGFR-2 receptor

https://doi.org/10.1021/acsomega.2c05206
ACS Omega 2022, 7, 33614−33628

Table 6. 50% Inhibitory Concentration (IC_{50}, μM) of Active Compounds for DHFR and VEGFR-2 Inhibitory Activities[a]

compound	DHFR	VEGFR-2
5b	9.085 ± 0.511	0.623 ± 0.056
8b	7.881 ± 0.442	0.384 ± 0.047
methotrexate	0.022 ± 0.008	ND
sorafenib	ND	0.069 ± 0.021

[a]ND, not determined; IC_{50} ± SEM (μM, SEM—standard error of the mean).

than the DHFR receptor. Furthermore, many naphthamide derivatives have also shown highly selective and strong VEGFR-2 inhibitory activity in some published studies.[12,23,28] Therefore, the study results may suggest that the potent anticancer activity of our active compounds is mediated by interaction with the VEGFR-2 protein.

4. CONCLUSIONS

In summary, 10 novel 2-naphthamide derivatives have been designed, synthesized, and evaluated for their antimicrobial and anticancer activities. The reaction yield was greatly increased as well as the reaction time was significantly reduced using a microwave-assisted method. Compound **8b** showed potent antibacterial activity against five strains EC, SF, SE, MSSA, and MRSA with MIC ranging between 8 and 16 μg/mL as compared to ciprofloxacin. Moreover, compounds **5b** and **8b** also exhibited potent anticancer activity with IC_{50} < 8.5 μM against C26, HepG2, and MCF7 cell lines compared with the reference drug PTX. From the structure−activity relationship, the presence of the *N*-(4-methyl/4-chlorobenzyl), 4-hydroxy, and 5,7-dimethoxy groups of the 2-naphthamide scaffold is more desirable for enhanced antibacterial and antitumor activities in **5b** and **8b**. Molecular docking predicted that DHFR and VEGFR-2 proteins from *Escherichia coli* are the most suitable targets for antibacterial and anticancer activities. Compound **8b** being the most potent anticancer displayed good interactions against DHFR and VEGFR-2 with the affinity of −9.8 Kcal/mol as compared with PTX (−9.9 Kcal/mol at DHFR and −8.2 Kcal/mol at VEGFR-2). Moreover, compound **8b** showed excellent *in vitro* VEGFR-2 inhibitory activity with the IC_{50} value of 0.384 μM compared with the positive control sorafenib (IC_{50} = 0.069 μM). The obtained ADMET results suggest that these derivatives showed a good ADMET profile. This work paved the way for the synthesis of more potent compounds based on 2-naphthamide scaffolds and explored their various potential biological activities as well as their mechanism of action.

■ ASSOCIATED CONTENT

Supporting Information

The Supporting Information is available free of charge at https://pubs.acs.org/doi/10.1021/acsomega.2c05206.

Docking Information for the most active compounds ^{1}H and ^{13}C NMR spectra for all new compounds (PDF)

■ AUTHOR INFORMATION

Corresponding Authors

Em Canh Pham − *Department of Medicinal Chemistry, Faculty of Pharmacy, Hong Bang International University, 700000 Ho Chi Minh City, Vietnam;* orcid.org/0000-0002-0160-336X; Email: canhem112009@gmail.com, empc@hiu.vn

Tuyen Ngoc Truong − *Department of Organic Chemistry, Faculty of Pharmacy, University of Medicine and Pharmacy at Ho Chi Minh City, 700000 Ho Chi Minh City, Vietnam;* orcid.org/0000-0002-0952-1633; Email: truongtuyen@ump.edu.vn

Complete contact information is available at: https://pubs.acs.org/10.1021/acsomega.2c05206

Author Contributions

E.C.P.: Conceptualization, methodology, investigation, software, data curation, supervision, writing—original draft preparation; writing—review and editing. T.N.T.: Data curation, supervision, writing—original draft preparation, writing—review and editing.

Notes

The authors declare no competing financial interest.

■ ACKNOWLEDGMENTS

This work was supported by the Hong Bang International University [grant numbers GVTC15.22, 2022].

■ REFERENCES

(1) Em, P. C.; Tuong Vi, L. T.; Long, T. P.; Huong-Giang, T. N.; Khanh, N. B. L.; Tuyen, N. T. Design, synthesis, antimicrobial evaluations and *in silico* studies of novel pyrazol-5(4*H*)-one and 1*H*-pyrazol-5-ol derivatives. *Arab. J. Chem.* **2022**, *15*, No. 103682.

(2) Fisher, M. C.; Alastruey-Izquierdo, A.; Berman, J.; Bicanic, T.; Bignell, E. M.; Bowyer, P.; Bromley, M.; Brüggemann, R.; Garber, G.; Cornely, O. A.; Gurr, S. J.; Harrison, T. S.; Kuijper, E.; Rhodes, J.; Sheppard, D. C.; Warris, A.; White, P. L.; Xu, J.; Zwaan, B.; Verweij, P. E. Tackling the emerging threat of antifungal resistance to human health. *Nat. Rev. Microiol.* **2022**, *20*, 557−571.

(3) Antimicrobial Resistance Collaborators; Ikuta, K. S.; Sharara, F.; et al. Global burden of bacterial antimicrobial resistance in 2019: a systematic analysis. *Lancet* **2022**, *399*, 629−655.

(4) Ward, R. A.; Fawell, S.; Floc'h, N.; Flemington, V.; McKerrecher, D.; Smith, P. D. Challenges and opportunities in cancer drug resistance. *Chem Rev.* **2021**, *121*, 3297−3351.

(5) Cellupica, E.; Pantalone, S.; Papagni, F.; Rui, M.; Siciliano, A. M.; Collina, S.; et al. Vinca alkaloids and analogues as anti-cancer agents: Looking back, peering ahead. *Bioorg. Med. Chem. Lett.* **2018**, *28*, 2816−2826.

(6) Mosca, L.; Ilari, A.; Fazi, F.; Assaraf, Y. G.; Colotti, G. Taxanes in cancer treatment: Activity, chemoresistance and its overcoming. *Drug Resist Updat.* **2021**, *54*, No. 100742.

(7) Ibrahim, S. R. M.; Mohamed, G. A. Naturally occurring naphthalenes: chemistry, biosynthesis, structural elucidation, and biological activities. *Phytochem. Rev.* **2016**, *15*, 279−295.

(8) Devkota, L.; Lin, C. M.; Strecker, T. E.; Wang, Y.; Tidmore, J. K.; Chen, Z.; Guddneppanavar, R.; Jelinek, C. J.; Lopez, R.; Liu, L.; Hamel, E.; Mason, R. P.; Chaplin, D. J.; Trawick, M. L.; Pinney, K. G. Design, synthesis, and biological evaluation of water-soluble amino acid prodrug conjugates derived from combretastatin, dihydronaphthalene, and benzosuberene-based parent vascular disrupting agents. *Bioorg. Med. Chem.* **2016**, *24*, 938−956.

(9) Wang, G.; Liu, W.; Fan, M.; He, M.; Li, Y.; Peng, Z. Design, synthesis and biological evaluation of novel thiazole-naphthalene derivatives as potential anticancer agents and tubulin polymerisation inhibitors. *J. Enzyme Inhib. Med. Chem.* **2021**, *36*, 1694−1702.

(10) Wei, M.; Peng, X.; Xing, L.; Dai, Y.; Huang, R.; Geng, M.; Zhang, A.; Ai, J.; Song, Z. Design, synthesis and biological evaluation of a series of novel 2-benzamide-4-(6-oxy-*N*-methyl-1-naphthamide)-pyridine derivatives as potent fibroblast growth factor receptor (FGFR) inhibitors. *Eur. J. Med. Chem.* **2018**, *154*, 9−28.

(11) Wang, G.; Qiu, J.; Xiao, X.; Cao, A.; Zhou, F. Synthesis, biological evaluation and molecular docking studies of a new series of chalcones

containing naphthalene moiety as anticancer agents. *Bioorg. Chem.* **2018**, *76*, 249−257.
(12) Lv, Y.; Li, M.; Cao, S.; Tong, L.; Peng, T.; Wei, L.; Xie, H.; Ding, J.; Duan, W. Discovery of anilinopyrimidine-based naphthamide derivatives as potent VEGFR-2 inhibitors. *Med. Chem. Commun.* **2015**, *6*, 1375.
(13) Voskienė, A.; Sapijanskaitė, B.; Mickevičius, V.; Jonuškienė, I.; Stasevych, M.; Komarovska-Porokhnyavets, O.; Musyanovych, R.; Novikov, V. Synthesis and microbiological evaluation of new 2- and 2,3-diphenoxysubstituted naphthalene-1,4-diones with 5-oxopyrrolidine moieties. *Molecules* **2012**, *17*, 14434−14448.
(14) Wang, Y.; Mowla, R.; Ji, S.; Guo, L.; De Barros Lopes, M. A.; Jin, C.; Song, D.; Ma, S.; Venter, H. Design, synthesis and biological activity evaluation of novel 4-subtituted 2-naphthamide derivatives as AcrB inhibitors. *Eur. J. Med. Chem.* **2018**, *143*, 699−709.
(15) Sirgamalla, R.; Kommakula, A.; Banoth, S.; Dharavath, R.; Adem, K.; Palithepu, M.; Boda, S.; Premkumar, K. Design, synthesis and biological evaluation of novel *N*1,*N*8-bis(((4-((5-aryl-1,3,4-oxadiazol-2-yl)methoxy)phenyl)amino)oxy)-1-naphthamide derivatives. *Synth. Commun.* **2018**, *48*, 954−962.
(16) Altıntop, M. D.; Atlı, Ö.; Ilgın, S.; Demirel, R.; Özdemir, A.; Kaplancıklı, Z. A. Synthesis and biological evaluation of new naphthalene substituted thiosemicarbazone derivatives as potent antifungal and anticancer agents. *Eur. J. Med. Chem.* **2016**, *108*, 406−414.
(17) An, Y.; Dong, Y.; Liu, M.; Han, J.; Zhao, L.; Sun, B. Novel naphthylamide derivatives as dual-target antifungal inhibitors: Design, synthesis and biological evaluation. *Eur. J. Med. Chem.* **2021**, *210*, No. 112991.
(18) Chen, Y. J.; Huang, S. M.; Tai, M. C.; Chen, J. T.; Lee, A. R.; Huang, R. Y.; Liang, C. M. The anti-fibrotic and anti-inflammatory effects of 2,4-diamino-5-(1-hydroxynaphthalen-2-yl)-5*H*-chromeno-[2,3-b]pyriine-3-carbonitrile in corneal fibroblasts. *Pharmacol. Rep.* **2020**, *72*, 115−125.
(19) Shirinzadeh, H.; Ghalia, M.; Tascioglu, A.; Adjali, F. I.; Gunesacar, G.; Gurer-Orhan, H.; Suzen, S. Bioisosteric modification on melatonin: synthesis of new naphthalene derivatives, *in vitro* antioxidant activity and cytotoxicity studies. *Braz. J. Pharm. Sci.* **2020**, *56*, No. e18124.
(20) Goldstein, M.; Goodey, N. M. Distal Regions regulate dihydrofolate reductase-ligand interactions. *Methods Mol. Biol.* **2021**, *2253*, 185−219.
(21) Simons, M.; Gordon, E.; Claesson-Welsh, L. Mechanisms and regulation of endothelial VEGF receptor signalling. *Nat. Rev. Mol. Cell Biol.* **2016**, *17*, 611−625.
(22) Cheng, K.; Liu, C. F.; Rao, G. W. Anti-angiogenic agents: A review on vascular endothelial growth factor receptor-2 (VEGFR-2) inhibitors. *Curr. Med. Chem.* **2021**, *28*, 2540−2564.
(23) Harmange, J. C.; Weiss, M. M.; Germain, J.; Polverino, A. J.; Borg, G.; Bready, J.; Chen, D.; Choquette, D.; Coxon, A.; DeMelfi, T.; DiPietro, L.; Doerr, N.; Estrada, J.; Flynn, J.; Graceffa, R. F.; Harriman, S. P.; Kaufman, S.; La, D. S.; Long, A.; Martin, M. W.; Neervannan, S.; Patel, V. F.; Potashman, M.; Regal, K.; Roveto, P. M.; Schrag, M. L.; Starnes, C.; Tasker, A.; Teffera, Y.; Wang, L.; White, R. D.; Whittington, D. A.; Zanon, R. Naphthamides as novel and potent vascular endothelial growth factor receptor tyrosine kinase inhibitors: design, synthesis, and evaluation. *J. Med. Chem.* **2008**, *51*, 1649−1667.
(24) Pham, E. C.; Tuyen, T. N.; Nguyen, D. H.; Duy, V. D.; Hong Tuoi, D. T. Synthesis of a series of novel 2-amino-5-substituted 1,3,4-oxadiazole and 1,3,4-thiadiazole derivatives as potential anticancer, antifungal and antibacterial agents. *Med. Chem.* **2022**, *18*, 558−573.
(25) Xiong, G.; Wu, Z.; Yi, J.; Fu, L.; Yang, Z.; Hsieh, C.; Yin, M.; Zeng, X.; Wu, C.; Lu, A.; Chen, X.; Hou, T.; Cao, D. ADMETlab 2.0: an integrated online platform for accurate and comprehensive predictions of ADMET properties. *Nucleic Acids Res.* **2021**, *49*, W5−W14.
(26) Em, P. C.; Lenh, V. V.; Cuong, V. N.; Ngoc Thoi, N. D.; Tuong Vi, L. T.; Tuyen, N. T. *In vitro* and *in vivo* antidiabetic activity, isolation of flavonoids, and *in silico* molecular docking of stem extract of *Merremia tridentata* (L.). *Biomed. Pharmacother.* **2022**, *146*, No. 112611.
(27) Pham, E. C.; Tuong Vi, L. T.; Tuyen, N. T. Design, synthesis, bio-evaluation, and in silicostudies of some N-substituted 6-(chloro/nitro)-1H-benzimidazole derivatives as antimicrobial and anticancer agents. *RSC Adv.* **2022**, *12*, 21621−21646.
(28) Li, M. Y.; Lv, Y. C.; Tong, L. J.; Peng, T.; Qu, R.; Zhang, T.; Sun, Y. M.; Chen, Y.; Wei, L. X.; Geng, M. Y.; Duan, W. H.; Xie, H.; Ding, J. DW10075, a novel selective and small-molecule inhibitor of VEGFR, exhibits antitumor activities both *in vitro* and *in vivo*. *Acta Pharmacol. Sin.* **2016**, *37*, 398−407.

https://doi.org/10.1021/acsomega.2c05206
ACS Omega 2022, 7, 33614−33628